AD-A125 392 CALCULATION AND MEASUREMENT OF SEPARATED TURBULENT BOUNDARY LAYERS(U) ROYAL AIRCRAFT ESTABLISHMENT FARNBOROUGH (ENGLAND) P D SMITH ET AL. OCT 82 1/1

UNCLASSIFIED RAE-TM-AERO-1955 DRIC-BR-86356 F/G 20/4 NL

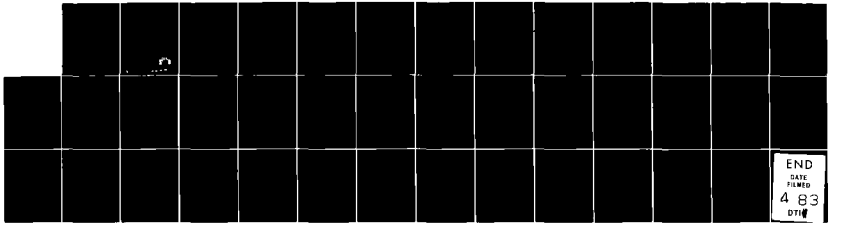

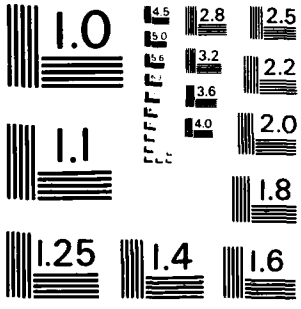

MICROCOPY RESOLUTION TEST CHART

NATIONAL BUREAU OF STANDARDS - 1963 - A

TECH. MEMO
AERO 1955

UNLIMITED

TECH.- MEMO
AERO 1955

ROYAL AIRCRAFT ESTABLISHMENT

CALCULATION AND MEASUREMENT OF SEPARATED TURBULENT BOUNDARY LAYERS

by

P. D. Smith
R. C. Hastings
B. R. Williams

October 1982

ROYAL AIRCRAFT ESTABLISHMENT

Technical Memorandum Aero 1955

Received for printing 15 October 1982

CALCULATION AND MEASUREMENT OF SEPARATED TURBULENT BOUNDARY LAYERS

by

P. D. Smith

R. C. Hastings

B. R. Williams

SUMMARY

An inverse integral prediction method for the development of separated turbulent boundary layers developed from the lag-entrainment method is described. The inverse method uses the concept of equilibrium separated boundary layer flows and the predicted characteristics of such flows will be compared with measurements which represent the first known demonstration that equilibrium separated boundary layers can be realised experimentally.

In these experiments the data were obtained with a single-component laser Doppler anemometer usually set up to measure streamwise components of mean velocity and turbulence intensity; in addition, however, one pair of profiles of the mean velocity and turbulence intensity normal to the wall was obtained. Shear stresses were not measured but values estimated using the data in conjunction with the differential momentum equation are shown and compared with the patterns already revealed by earlier work on attached equilibrium flows.

The separated flow on a NACA 4412 aerofoil has been measured by Wadcock using the flying hot-wire technique. The measured displacement thickness is used as input to the inverse prediction method. It is shown that predicted values of momentum thickness agree with the measured values but that the calculation predicts a pressure rise in the separated region whereas the pressure is almost constant in the experiment. The result of introducing second order effects into the calculation is shown. The equivalent inviscid flow is constructed and the matching of the equivalent and real flows is considered.

Paper presented at Euromech 148 Two-Dimensional Separated Flows, Bochum, W. Germany, 13-15 October 1981

LIST OF CONTENTS

		Page
1	THE INVERSE MODE OF THE LAG-ENTRAINMENT METHOD	3
2	CHARACTERISTICS OF SEPARATED EQUILIBRIUM BOUNDARY LAYERS	4
3	MEASUREMENTS IN AN EQUILIBRIUM SEPARATED BOUNDARY LAYER	5
4	CALCULATIONS OF SEPARATED FLOW ON A TWO-DIMENSIONAL AEROFOIL	8
	4.1 Calculation of the development of the boundary layer	8
	4.2 Matching of the inviscid and viscous flows	10
Table 1		13
References		14
Illustrations		Figures 1-23
Report documentation page		inside back cover

THE INVERSE MODE OF THE LAG-ENTRAINMENT METHOD

The standard direct mode of the lag-entrainment method computes the boundary layer development for given starting conditions and a specified externally imposed pressure gradient. East, Smith and Merryman[1] have developed an inverse mode of this process in which the pressure distribution is predicted for a given displacement surface. To do this they inverted the standard equations to obtain an expression for the pressure gradient parameter $(\theta/U_e)(dU_e/dx)$ as a function of the gradient of the displacement thickness, $d\delta^*/dx$ and other local parameters, *ie*

$$\frac{\theta}{U_e}\frac{dU_e}{dx} = \frac{1}{F_2}\left(\frac{d\delta^*}{dx} - F_1\right) \tag{1}$$

where $F_1 = H\frac{C_f}{2} + (1 + 0.2rM^2)\left(C_E - H_1\frac{C_f}{2}\right)\frac{d\bar{H}}{dH_1}$,

$$F_2 = -H(H + 2 - M^2) + (1 + 0.2rM^2)(H + 1)H_1\frac{d\bar{H}}{dH_1} + 0.4rM^2(1 + 0.2M^2)(\bar{H} + 1) ,$$

and

$$H = \frac{\delta^*}{\theta} , \qquad H_1 = \frac{(\delta - \delta^*)}{\theta} , \qquad H + 1 = (\bar{H} + 1)(1 + 0.2M^2) ,$$

C_f is the skin friction coefficient,

C_E is the entrainment coefficient.

As written by East *et al*, equation (1) is singular when $(dH_1/d\bar{H}) = 0$ but this is easily overcome by writing (1) as

$$\frac{\theta}{U_e}\frac{dU_e}{dx} = \frac{1}{F_2'}\left(\frac{dH_1}{d\bar{H}}\frac{d\delta^*}{dx} - F_1'\right) \tag{2}$$

where $F_2' = \frac{dH_1}{d\bar{H}}F_2$ and $F_1' = \frac{dH_1}{d\bar{H}}F_1$.

Lock[2] has pointed out that for interactive calculations involving an iteration between a boundary layer calculation and an inviscid flow calculation the use of a source strength Σ rather than δ^* is to be preferred.

Here

$$\Sigma = \frac{1}{\rho}\frac{d(\rho U_e\delta^*)}{dx} , \qquad ie \quad \frac{d\delta^*}{dx} = \Sigma - \frac{H\theta}{U_e}\frac{dU_e}{dx}(1 - M^2)$$

so that

$$\frac{\theta}{U_e}\frac{dU_e}{dx} = \frac{1}{F_3'}\left(\frac{dH_1}{d\bar{H}}\Sigma - F_1'\right) \tag{3}$$

where $F_3' = F_2' + H(1 - M^2)\frac{dH_1}{d\bar{H}}$.

2 CHARACTERISTICS OF SEPARATED EQUILIBRIUM BOUNDARY LAYERS

Equilibrium flows are defined in the lag-entrainment method as flows in which the shape of the velocity and shear stress profiles in the boundary layer do not vary with x. The parameters used to characterise compressible equilibrium flows are

$$G = \frac{\bar{H} - 1}{\bar{H}} \sqrt{\frac{2}{C_f}}$$

and

$$\pi = - \frac{2\delta^*}{C_f} \frac{1}{U_e} \frac{dU_e}{dx}$$

which are related by an equilibrium locus of the form

$$G = 6.432 \left[(1 + 0.8\pi)(1 + 0.04M^2) \right]^{\frac{1}{2}} \quad . \tag{4}$$

Equation (4) may be expressed in a form more suitable for separated flows (negative C_f) as

$$\frac{0.02417}{(1 + 0.04M^2)} = \frac{1}{G^2} - 0.8 \frac{\pi}{G^2} \quad . \tag{5}$$

The growth of the equilibrium boundary layer can be calculated by solving the momentum integral equation for a velocity distribution of the form

$$U_e \propto x^m \tag{6}$$

which defines the pressure gradient parameter, m, as

$$m = \frac{x}{U_e} \frac{dU_e}{dx} \quad . \tag{7}$$

The momentum integral equation for two-dimensional compressible flow is

$$\frac{d\theta}{dx} + (H + 2 - M^2) \frac{\theta}{U_e} \frac{dU_e}{dx} = \frac{C_f}{2} \tag{8}$$

hence for equilibrium flow

$$\frac{d\theta}{dx} + (H + 2 - M^2) \frac{m\theta}{x} = \frac{C_f}{2} \quad . \tag{9}$$

As H and C_f are assumed constant, equation (9) can be solved analytically if M is also assumed independent of x. Strictly such an assumption is not consistent with equation (6) but it is a valid approximation over a limited length of boundary-layer

development during which the change in M^2 is small compared with $(H + 2 - M^2)$. Integrating equation (9) gives

$$\frac{\theta}{x} = \frac{C_f}{2\left[1 + m(H + 2 - M^2)\right]} \quad . \tag{10}$$

Hence for these flows θ and δ^* (since H is constant) vary linearly with x. Substituting equations (10) and (7) into equation (5) together with an appropriate skin friction relationship enables an explicit expression for m to be obtained as a function of R_θ and H. This function is portrayed in Fig 1. In general for any given value of m two equilibrium flows are possible, one separated and the other attached although for $m \leqslant -0.2$ two attached solutions occur.

3 MEASUREMENTS IN AN EQUILIBRIUM SEPARATED BOUNDARY LAYER

In order that predicted and measured characteristics of equilibrium separated flow could be compared, an experiment was set up in the boundary layer tunnel at RAE Bedford. In this tunnel the test boundary layer is the one which grows on the flat ceiling of the working section and it can be subjected to a variety of pressure gradients by altering the shape of the flexible floor of the tunnel. Equilibrium attached boundary layers had previously been generated and studied in this way[3] in the tunnel.

In this instance, the requirement was for a configuration that would permit a separated boundary layer, whose external velocity (U_e) varied with distance according to a negative power law, to form along part of the ceiling at the same time as there was a much thinner attached boundary layer on the floor. This was achieved with the arrangement shown diagrammatically in Fig 2. Vortex generators were used to inhibit the growth of the boundary layers on the tunnel's side walls and a bleed slot was inserted at a joint in the tunnel floor to thin the floor boundary layer.

The main instrumentation consisted of static pressure tappings along the centreline of the ceiling and a movable, single-channel, laser Doppler anemometer to measure velocity components parallel to the ceiling. The anemometer incorporated Bragg cells to introduce frequency shifts into its light beams so that the signs of the measured velocity components could be determined. In addition, the anemometer was temporarily adapted to measure vertical velocity components at one streamwise station along the working section.

The streamwise variation of pressure measured along the centreline of the ceiling is shown in Fig 3a and the extent of the ceiling and floor boundary layers in Fig 3b. The region of equilibrium flow, between an upstream zone of development toward equilibrium and a downstream zone in which the ceiling and floor boundary layers are believed to have been sufficiently close to interfere with each other is shown in Fig 3a.

In the equilibrium region, the pressure variation corresponds to

$$U_e \propto x^m$$

where $m = -0.122$ if x is measured from the virtual origin of the equilibrium boundary layer.

The displacement and momentum thicknesses (δ^*, θ) for the test boundary layer on the centreline of the ceiling are shown in Fig 4. This shows that the linear growth characteristic of equilibrium flow was achieved. Measurements offset 200 mm on either side of the centreline were also made. The offset momentum and displacement thicknesses agree with centreline values within about 8% and 10% respectively. The flow appears to be slightly asymmetrical with values to starboard agreeing better with the centreline values than those to port; the latter correspond to a slightly thinner boundary layer whose shape parameter H is between 1% and 10% lower than comparable centreline values.

The centreline measurements are consistent with the following boundary layer growth properties:

$$\frac{d\theta}{dx} = 0.0193 , \qquad \frac{d\delta^*}{dx} = 0.104 .$$

Consequently mean values of $H = \delta^*/\theta$ and $J = (H-1)/H$ are 5.38 and 0.814 respectively.

The experimental values $J = 0.814$ and $m = -0.122$ may be compared with the predicted (m,J) locus discussed in section 2, for which $m = -0.122$ gives $J = 0.839$. It will be seen that J does not fall on but below the predicted locus; in fact it is roughly as close to the locus as were the attached flow measurements of Ref 3.

Centreline profiles of streamwise velocity ratio U/U_e at a series of streamwise locations are shown in Fig 5. They exhibit an encouraging degree of similarity, though it has to be admitted that the streamwise length covered by the measurements is rather small.

Profiles near the wall are shown to expanded scales in Fig 6. There is no evidence that the universal law of the wall for attached flow, with an appropriately modified definition $(-\tau_w/\rho)^{\frac{1}{2}}$ of U_τ , can be applied to the reverse flow profile. This is because the maximum reversed velocities occur very close to the surface.

Fig 7 shows the only profile of the vertical velocity ratio V/U_e that was measured. The profile shape is generally consistent with two-dimensional equilibrium flow if U/U_e behaves as shown in Fig 5. However values of V/U_e are rather too large in general.

Normalised, mean square, vertical and horizontal components of turbulence, $\overline{u^2}/U_e^2$ and $\overline{v^2}/U_e^2$, are shown in the next figure (Fig 8) for the one station where both are available. The distributions of these quantities may be compared with the corresponding distributions for a flow near separation (Flow 7) from Ref 3. Both components tend to peak near $y/\delta = 0.6$ for both flows, but the peaks for both components are rather more than twice as high in the separated flow as in the attached flow.

The ratio

$$\frac{1}{\theta}\int_0^\infty \frac{\overline{u^2} - \overline{v^2}}{U_e^2}\, dy \simeq 0.145$$

for the separated flow.

This indicates that normal Reynolds stress effects are considerably more important relative to shear stress effects in the momentum integral equation than would be expected on the basis of results for equilibrium attached flow. It is found for the latter in Ref 3 that the ratio is always about 0.072 J so that the expected value would be about 0.059 for $J = 0.814$.

Since the shear stress distribution across the separated boundary layer was not measured, it was thought worthwhile to estimate it. This was done in the following way. It was assumed that viscous effects would be important only in a tiny region close to the surface and could be neglected. On this premise it was further assumed that: the velocity profiles at different streamwise locations would have the same shape (that is U/U_e would be a function of y/δ only), $\delta \propto x$, and $U_e \propto x^m$, if x is measured from the virtual origin of the equilibrium layer. These assumptions enable the differential equation of boundary layer motion to be reduced to an ordinary differential equation if it is also assumed that the shear stress term $-\overline{UV}$ is expressible as the product of a function of y/δ and a factor proportional to x^{2m} . The differential equation developed in this way was integrated numerically to find the shear distribution, with appropriate experimental information fed in, and the starting condition that the shear was zero at the surface. This condition had the advantage that no assumed value of skin friction coefficient (C_f) was required to start the calculation but meant that the computed estimate of $\tau/\rho U_e^2$ should tend to $-C_f/2$ rather than zero at the edge of the boundary layer.

Two basic calculations were performed: a first approximation to the shear distribution was obtained by assuming that static pressure was constant across the thickness of the boundary layer, and a second approximation in which $\partial P/\partial y = -(\partial \rho \overline{V^2}/\partial y)$ and the effect of the term $\partial \overline{U^2}/\partial x$ on the streamwise momentum balance was included. Results are shown in Fig 9. The first approximation yielded a shear stress distribution with a relatively high peak and thereafter a fairly sharp decay. The value outside the boundary layer was negative and not the small positive value to be expected. Taking a second approximation produced a slightly lower peak followed by a more gradual and plausible decay; however values outside the boundary layer appeared to be too high.

An additional case was computed in which the input values of $\partial\delta/\partial x$ and $|m|$ were respectively increased and decreased by 2.7%. This case, too, is shown in Fig 9. The residual shear at the outer edge of the boundary layer was halved. The 2.7% changes illustrated had no appreciable effect on the shear stress estimate for the inner two-thirds of the boundary layer. The estimate for the inner third is almost linear and clearly the relation $\partial P/\partial x = \partial \tau/\partial y$, valid at $y = 0$, is the dominant influence on the profile in that region.

The next figure, Fig 10, shows some shear stress distributions taken from the attached-flow measurements of Ref 3. The figure shows how the maximum normalised shear stress both moves away from the surface and increases in magnitude as separation is approached. The shear stress estimates for the separated flow are plausible in general terms, in that they indicate that the trend continues.

All in all, the experiment on the one separated flow with an adverse pressure gradient, which it has so far been possible to set up, confirms that the concept of equilibrium separated flow is valid; however detailed examination of the measurements indicate that the flow studied is not truly in two-dimensional equilibrium. The profile of V/U_e is not completely consistent with the U/U_e profile and the gradient of the latter, outside the boundary layer (this may just be discerned in Fig 5) is rather too large to be compatible with the growth of the displacement thickness. Furthermore, the velocity component profiles, surface pressure gradient and boundary layer growth do not lead to completely satisfactory estimates of shear stress. The importance of second-order effects in this boundary layer is noteworthy; it may be that third order effects are not completely negligible.

4 CALCULATIONS OF SEPARATED FLOW ON A TWO-DIMENSIONAL AEROFOIL

The use of the inverse boundary-layer method developed by East *et al*[1] is demonstrated by calculating the development of the separated flow at the trailing edge of a NACA 4412 aerofoil, using the measurements of Wadcock[4] for the boundary conditions. Having demonstrated the ability of the inverse boundary layer method to calculate this class of flow, the flow about the complete aerofoil is calculated by matching an external inviscid incompressible flow with the inverse boundary layer by the scheme developed by Le Balleur[5] and further described by Lock[2]. It is shown that the solutions converge for examples with separating and separated flow at the trailing edge.

4.1 Calculation of the development of the boundary layer

Measurements by a flying hot-wire of the separated flow on a NACA 4412 aerofoil at 13.87° incidence have been reported by Wadcock[4]. The displacement thickness measured by Wadcock has been used as input to the inverse lag entrainment method. It is shown that the predicted values of momentum thickness and shape factor agree with the measured values, but the predicted values of the velocity do not agree with the measured values. It is demonstrated that quite large changes in the displacement thickness produce only small changes in the predicted values, thus the disagreement cannot be explained by errors in the measurements in the experiment. However a change in the $H \sim H_1$ relationship produces a marked change in the predicted velocities, which suggests that some future work is required to derive an appropriate $H \sim H_1$ relationship. To allow an exploration of a fuller range of $H \sim H_1$ relationship the form of the lag entrainment equations suggested by Lock[2] is used so they can be integrated through the singularity which occurs in the form given by East *et al*[1] if $dH_1/dH = 0$. It should be noted that the predicted velocities must be corrected for second order effects before they can be compared with the measured velocities. East[6] has pointed out that in a proper second order treatment of the momentum integral equation the velocity distribution from the equivalent inviscid flow should be used rather than the distribution from the real viscous flow. By the converse argument it follows that the inverse boundary layer equation will predict the velocity in the equivalent inviscid flow. At separation the second order terms are important which will give a significant difference between the equivalent and real flows. An attempt is made to quantify these differences and perform a valid comparison of the measured and predicted velocity distributions.

The experimental data used in these calculations are given in Table 1. The surface velocities are interpolated from the data in Wadcock's PhD thesis and the source strength is calculated by numerical differentiation. In Fig 11 the development of H is shown to compare well with the experimental values and an equally good agreement was obviously found for the momentum thickness. These calculations were performed with the $H \sim H_1$ relationship given by East *et al*[1],

$$\left.\begin{aligned} H_1 &= 4.5455 + 295 \exp(-3.325H) \\ \frac{d\bar{H}}{dH_1} &= -\frac{\exp(3.325\bar{H})}{980} \end{aligned}\right\} \quad \bar{H} > 1.6 \ . \qquad (11)$$

Results are also shown for a 'modified' East $H - H_1$ relationship in which $0.01\ (\bar{H}-1)^2$ has been subtracted from the expression for H_1. This results in a reduction in the coefficient, $d\bar{H}/dH_1$ in the differential equation for H and consequentially a slower growth of H.

The velocity distribution predicted by the inverse boundary layer method is given in Fig 12 for both $H - H_1$ relationships. There is a marked disagreement between the predicted and measured values, with the predicted velocities decreasing throughout the separated region.

It is possible that the displacement thickness was measured incorrectly. However an increase in the displacement thickness by 35%, which should exceed any experimental error, only increased the velocity at the trailing edge by 0.02 whilst the difference between equivalent and real flows is 0.135 as shown in Fig 12.

By integrating the normal momentum equation Lock[2] shows that, to second order, the difference between the pressure at the wall in the equivalent inviscid flow, P_{iw} and the pressure in the real viscous flow, P_w is given by

$$P_{iw} - P_w = \rho_{iw} U_{iw}^2 K^* (\theta + \bar{\delta}) \qquad (12)$$

where K^* is the curvature of the displacement surface. In Fig 13 this correction has been added to the equivalent inviscid flow and, bearing in mind the difficulty of evaluating the curvature accurately, there is reasonably good agreement with the real viscous flow up to separation. After separation the displacement surface is not curved and this correction has a negligible effect.

The effect of using different $H - H_1$ relationships was examined and the relationships are plotted in Fig 14 and are listed below: Green[7]

$$\left.\begin{aligned} H_1 &= 2 + 1.5\left(\frac{1.12}{H-1}\right)^{1.09289} + 0.5\left(\frac{H-1}{1.12}\right)^{1.09289} \\ \frac{dH_1}{dH} &= -1.85549(H-1)^{-2.09289} + 0.48279(H-1)^{0.09289} \ . \end{aligned}\right\} \qquad (13)$$

East[1]:

$$\left.\begin{aligned} H_1 &= 3.15 + \frac{1.72}{(H-1)} \\ \frac{dH}{dH_1} &= -\frac{(H-1)^2}{1.72} \end{aligned}\right\} \qquad H \leqslant 1.6 \ . \tag{14}$$

As equation (11) if $H > 1.6$.

The equations for the inverse method for incompressible flow take the form:

$$\frac{d\theta}{dx} = \frac{C_f}{2} - (H+2)\frac{\theta}{U}\frac{dU}{dx} \tag{15}$$

$$\frac{\theta}{U}\frac{dU}{dx} = \frac{1}{(H+1)}\left\{\frac{C_f}{2} - \frac{C_E - H_1\Sigma}{D}\right\} \tag{16}$$

$$\frac{dH}{dx} = \frac{1}{\theta}\frac{(H_1\Sigma - HC_E)}{D} \tag{17}$$

$$\frac{dC_E}{dx} = \frac{1}{\theta}F\left(C_{E_0}, C_{f_0}\right)\left[\frac{2.8}{H+H_1}\left\{(C_\tau)^{\frac{1}{2}}_{EQ_0} - \lambda C_\tau^{\frac{1}{2}}\right\} - \left(\frac{\theta}{U}\frac{dU}{dx}\right)_{EQ} - \frac{\theta}{U}\frac{dU}{dx}\right] \tag{18}$$

where the last equation is the 'lag equation' for C_E ,

$$D = H_1 - H\frac{dH_1}{dH}$$

which is never negative, and now the source strength Σ is regarded as 'known' and $(1/U)(dU/dx)$ as 'unknown'. It will be seen in section 5 that the source strength rather than the displacement thickness ties in with the scheme for matching the viscous and inviscid flows.

The results for the different $H \sim H_1$ relationships are indicated in Figs 11 and 12. The expression originally used by Green[7] produces a marked change in both the velocity and the development of H ; but neither of these changes appears very realistic and more experimental evidence is required to determine an appropriate $H \sim H_1$ relationship.

4.2 Matching of the inviscid and viscous flows

In the previous section it has been demonstrated that the boundary layer equations can be integrated through the singularity at separation if the equations are cast in inverse form for which prescribed values of the source strength Σ predict the velocity gradient parameter $(1/U)(dU/dx)$ (see equation (16)). It seems natural to use the solution of the inverse boundary layer equations as input to an inverse inviscid method to obtain a new estimate of the displacement surface (*ie* Σ). However it may be difficult to solve the inviscid problem since Motz[8] has indicated that there is a singularity in the inviscid flow at the point where the boundary conditions change from direct (shape

specified) to inverse (velocity specified), *ie* at the transition from calculations with the direct boundary layer method to the inverse form. This difficulty is overcome if the 'semi-inverse' technique as described by Carter[9], Le Balleur[5], Lock[2], Wigton and Holt[10] is adopted.

Such a technique is illustrated in Fig 15. An estimate of the source strength on the aerofoil and the sink strength in the wake is used to calculate (a) the inviscid velocity U^I_{iw} by a direct method, and (b) a velocity U^V_{iw} from the inverse boundary layer method. The two velocities are compared and if the scheme has not converged then the source strengths are updated by the formula

$$\Sigma^{n+1} = \Sigma^n + w \left[\frac{\theta}{U^V_{iw}} \frac{dU^V_{iw}}{dx} - \frac{\theta}{U^I_{iw}} \frac{dU^I_{iw}}{dx} \right]^{(n)} .$$

The analysis of Le Balleur[5] treats the error $\Sigma^n - \Sigma^\infty$ as a superposition of Fourier modes and this leads to an expression for the relaxation factor w, which for incompressible flow reduces to

$$w = \frac{B}{1 + B\theta\pi/\Delta x}$$

where Δx is the local step length and $B = (H+1)(H_1 - HdH/dH_1)/(dH/dH_1)$ which is the coefficient of $(\theta/U)(dU/dx)$ in the expression for the source strength derived from equation (16).

The direct inviscid solution for incompressible flow can be obtained by a panel method and in this case the symmetric-singularity model developed by Newling[11] is used. The initial development of the boundary layer is laminar and this is calculated directly by the method due to Thwaites[12]. The transition to a turbulent boundary layer can occur through natural transition which is predicted by Granvilles' criterion[13], or a laminar separation bubble predicted by Horton's method[14] or forced by a transition trip. The development of the turbulent boundary layer is calculated in either direct or inverse mode by the lag entrainment method. The turbulent boundary layer calculation can be switched from direct to inverse mode by any pre-determined criterion: for the following calculations the switch occurs when $H = 1.7$. The development of the combined wakes from the upper and lower surfaces is also calculated by the lag entrainment method, using the inverse mode. In the present calculations second order effects have not been included in either the calculation of the boundary layer or the construction of the equivalent inviscid flow. However following the method described by Lock[2] these effects can be included.

The method has been used to calculate the flow about a NACA 4412 aerofoil at a Reynolds number of 1.5×10^6. Transition was forced on the upper and lower surfaces at $x/c = 0.025$ and $x/c = 0.103$ respectively so that the results could be compared with the experiment described by Wadcock[4].

The first calculation was performed at an angle of incidence of 8° for which the flow is almost separating at the trailing edge. In Fig 16 it can be seen that the scheme converges to a lift coefficient slightly above the experimental value for a calculation with the semi-inverse technique applied on the upper surface wherever $H > 1.7$ and in the wake. A convergent solution is also produced if the semi-inverse technique is used for all the region occupied by the turbulent boundary layer on the upper surface. In Fig 17 the pressure distributions are compared and the theoretical results have a steeper adverse pressure gradient on the suction surface. In the previous section it was shown that a correction of the equivalent inviscid flow for curvature effects would reduce this difference. It should also be noted that passive flow control was added to Wadcock's experiment to obtain two-dimensional flow at 14° incidence. The same control was used at 8° incidence so the flow may not have been completely two-dimensional.

At an incidence of 14° the method again converges smoothly (see Fig 18) but the lift is now 5% above the experimental value. For the first nine iterations the flow is attached to the aerofoil but in Fig 19 it can be seen that the separation point moves forward as the number of iterations increases until it reaches $x/c = 0.918$. From Fig 20 the separation point in the experiment is further forward and most likely lies between $x/c = 0.70$ and $x/c = 0.75$. The theoretical method again predicts an adverse pressure gradient in the separated region and the difference in the pressure distribution in the separated region are a major contributor to the discrepancy in C_L shown in Fig 18.

The pressure distribution in the leading-edge region for the theory and the experiment are plotted in more detail in Fig 21. In the theoretical calculation there is a laminar separation bubble which reattaches ahead of the position of the transition trip in the experiment. Wadcock[4] did not detect any laminar separation bubble in the experiment. At the transition trip no increase in momentum thickness has been included in the calculation and this may explain the discrepancy in the development of momentum thickness shown in Fig 22. In Fig 23 there is a larger discrepancy in H and this behaviour ties in with the observed and predicted separation positions.

The semi-inverse scheme provides a method of obtaining converged solutions for flows with small regions of separated flow at the trailing edge. However the details of the calculation have not been in close agreement with the experiment of Wadcock. Although there is a reasonable agreement between the pressure distributions over the first 70% of the aerofoil there is not such good agreement in the boundary layer parameters over the same region. In the separated region there is a discrepancy in the measured and predicted pressures which was discussed in section 4.1.

In the future second order effects will be included in the boundary layer calculation and the matching of the inviscid and viscous flows and modifications to the $H \sim H_1$ relationship for the separated flow region will be investigated.

Table 1

EXPERIMENTAL DATA FOR NACA 4412 FROM WADCOCK

$\frac{x}{c}$ upper surface	U surface	δ^*	$\Sigma = \frac{1}{u}\frac{d}{dx}(U\delta^*)$
0.6292	1.275	0.0085	0.0482
0.6789	1.24	0.0112	0.0594
0.7267	1.218	0.0148	0.1006
0.7719	1.204	0.0210	0.1349
0.8142	1.194	0.0270	0.1738
0.8531	1.190	0.0354	0.2204
0.8880	1.187	0.0435	0.2262
0.9188	1.186	0.0504	0.2230
0.9949	1.186	0.0502	0.2268
0.9662	1.185	0.0612	0.2270
0.9823	1.182	0.0649	0.2152
0.9932	1.178	0.0674	0.2088
0.9986	1.175	0.0687	0.2095

REFERENCES

No.	Author	Title, etc
1	L.F. East P.D. Smith P.J. Merryman	Prediction of separated flows by the lag-entrainment method. RAE Technical Report 77046 (1977)
2	R.C. Lock M.C.P. Firmin	Survey of techniques for estimating viscous effects in external aerodynamics. IMA Conference on Numerical Methods in Aeronautical Fluid Dynamics, at Reading University, 30 March to 1 April 1981
3	L.F. East W.G. Sawyer C.R. Nash	An investigation of the structure of equilibrium turbulent boundary layers. RAE Technical Report 79040 (1979)
4	A.J. Wadcock	Flying-hot-wire study of two-dimensional turbulent separation on a NACA 4412 airfoil at maximum lift. PhD thesis, California Institute of Technology (1978)
5	J.C. Le Balleur	Couplage visqueux, non visqueux: methode numerique et applications aux ecoulement bidimensionnels transsoniques et supersoniques. La Recherche Aerospatiale No.2 (1978)
6	L.F. East	A representation of second-order boundary layer effects in the momentum integral equation and viscous-inviscid interactions. RAE Technical Report 81002 (1981)
7	J.E. Green	Application of Head's entrainment method to the prediction of turbulent boundary layers and wakes in compressible flow. RAE Technical Report 72079 (1972)
8	H. Motz	The treatment of singularities of partial differential equations by relaxation methods. Quart. Appl. Math. 4, pp.371-377 (1946)
9	J.E. Carter	A new boundary layer inviscid iteration technique for separated flow. AIAA Paper 79-1450 (1979)
10	L.B. Wigton M. Holt	Viscous-inviscid interaction in transonic flow. AIAA Paper 81-1003
11	J.C. Newling	An improved two-dimensional multi-aerofoil program. HSA-MAE-R-FDH-0007 (1977)
12	B. Thwaites (Ed)	Incompressible aerodynamics. Clarendon Press (1960)

REFERENCES (concluded)

No.	Author	Title, etc
13	P.S. Graville	The calculation of viscous drag of bodies of revolution. DTMB Report 849 (1953)
14	H.P. Horton	A semi-empirical theory for the growth and bursting of laminar separation bubbles. ARC CP 1073 (1967)

Reports quoted are not necessarily available to members of the public or to commercial organisations.

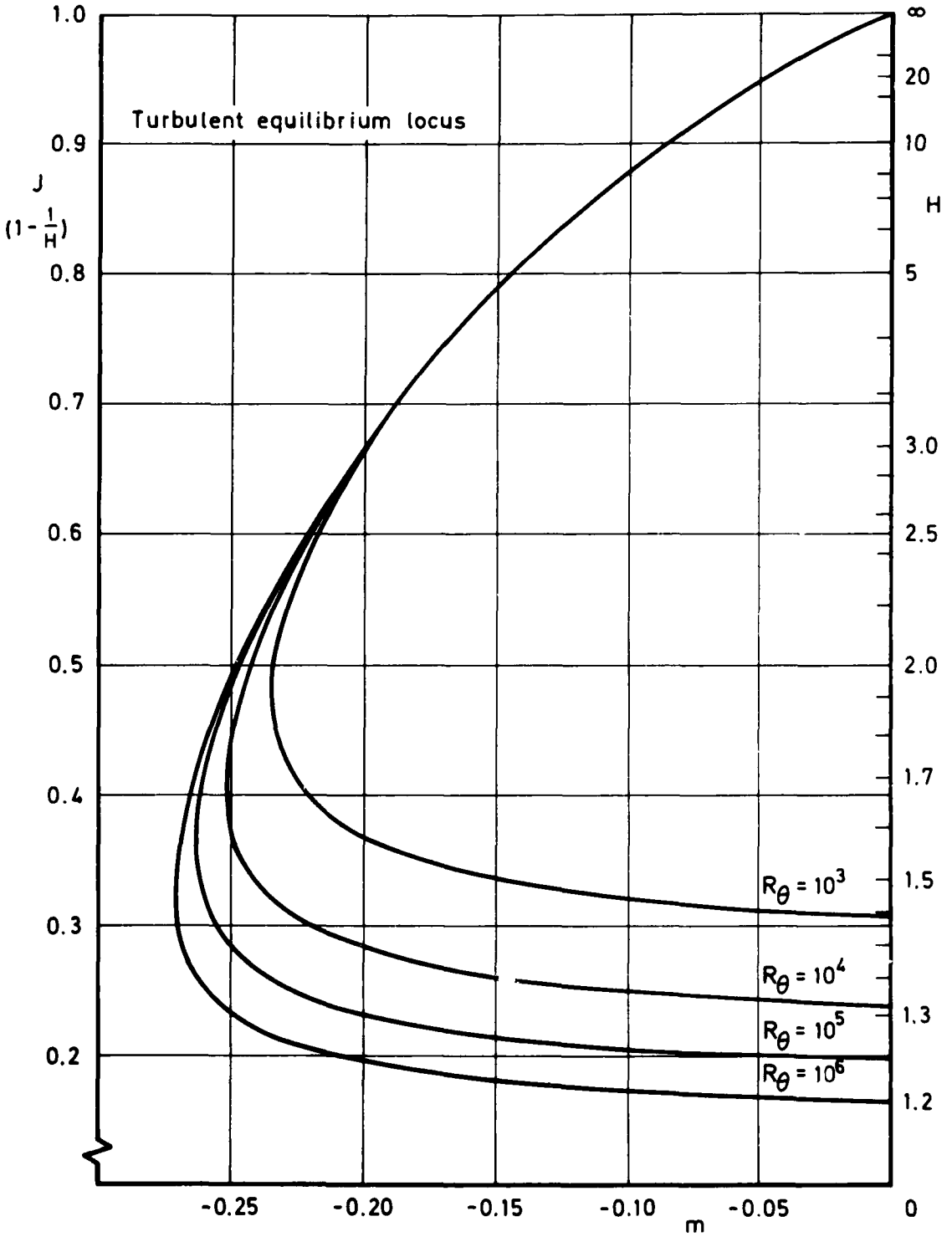

Fig 1 The shape parameter for equilibrium turbulent boundary layers

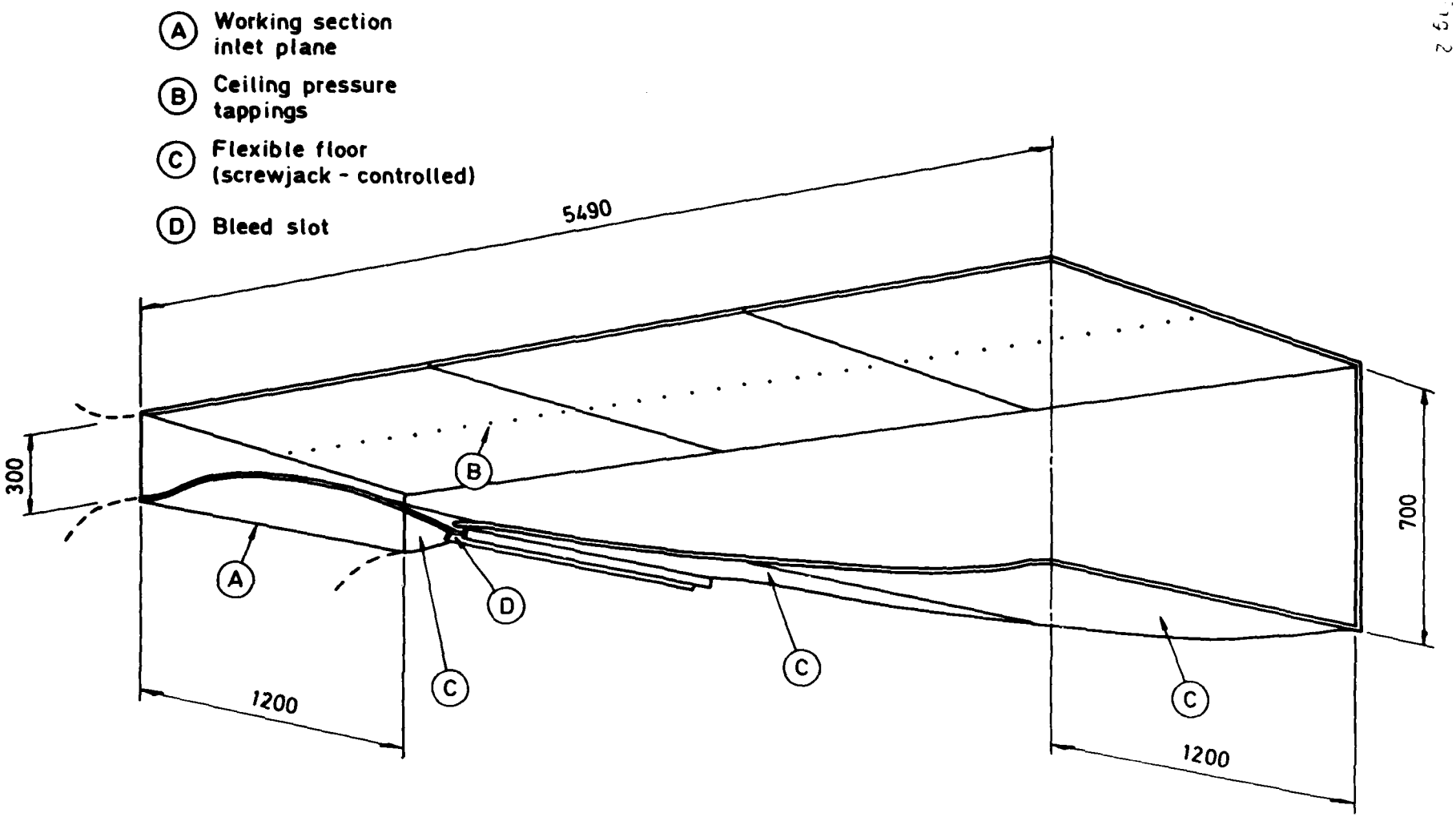

Fig 2 Diagrammatic view of boundary layer tunnel working section as seen from port side of outlet (port side wall omitted)

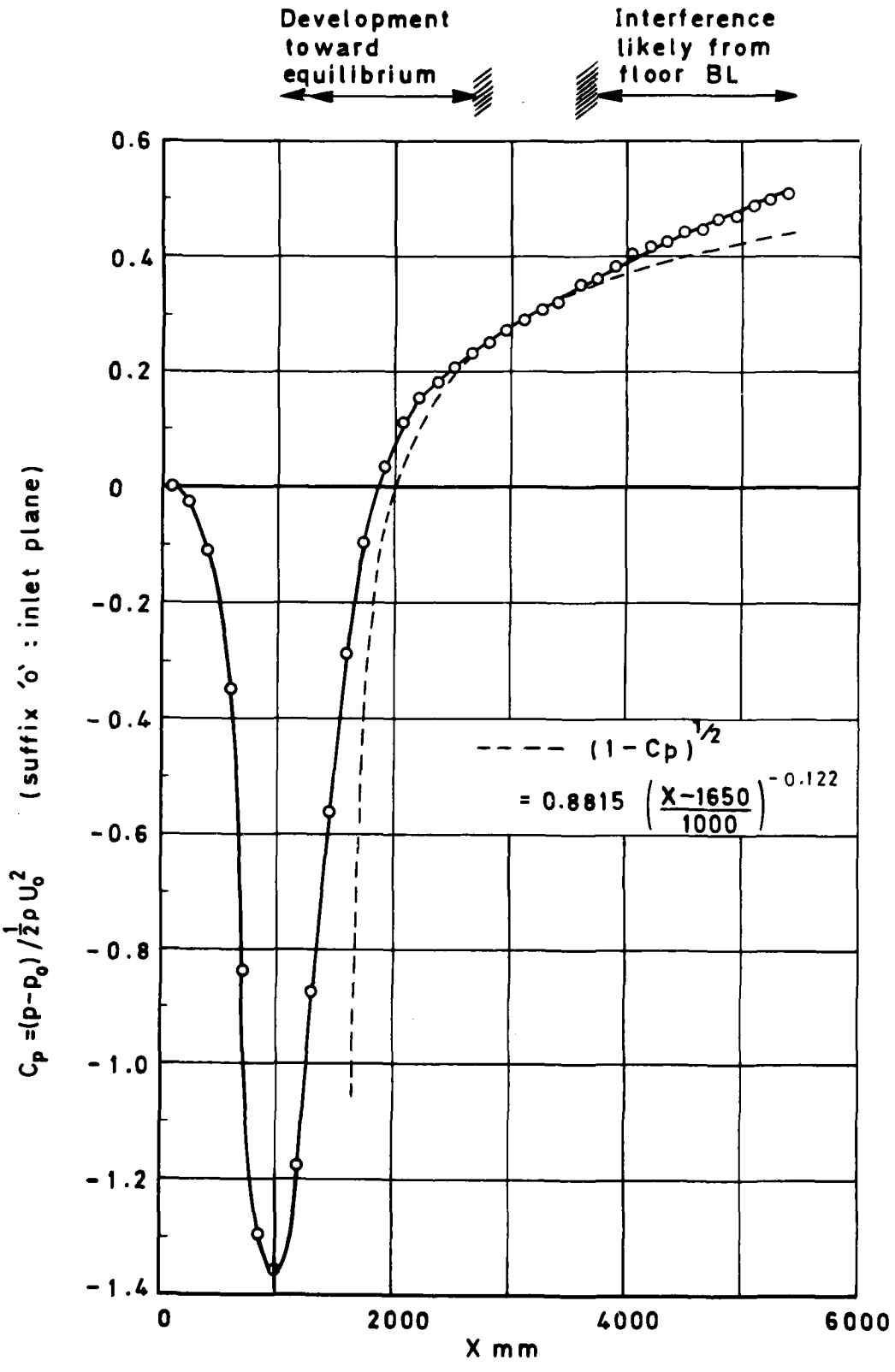

Fig 3a Ceiling pressure distribution

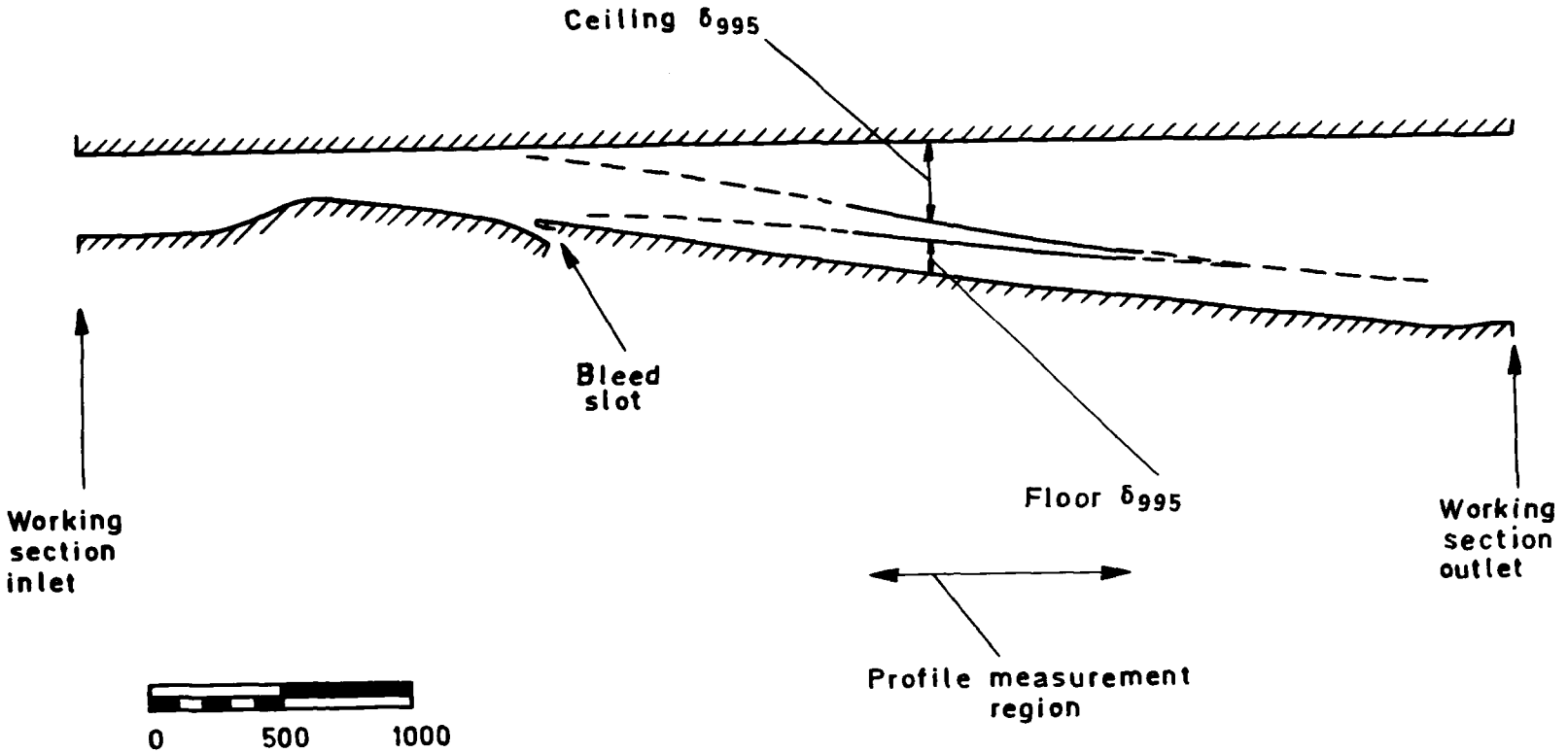

Fig 3b Working section in elevation with boundary layer growth indicated

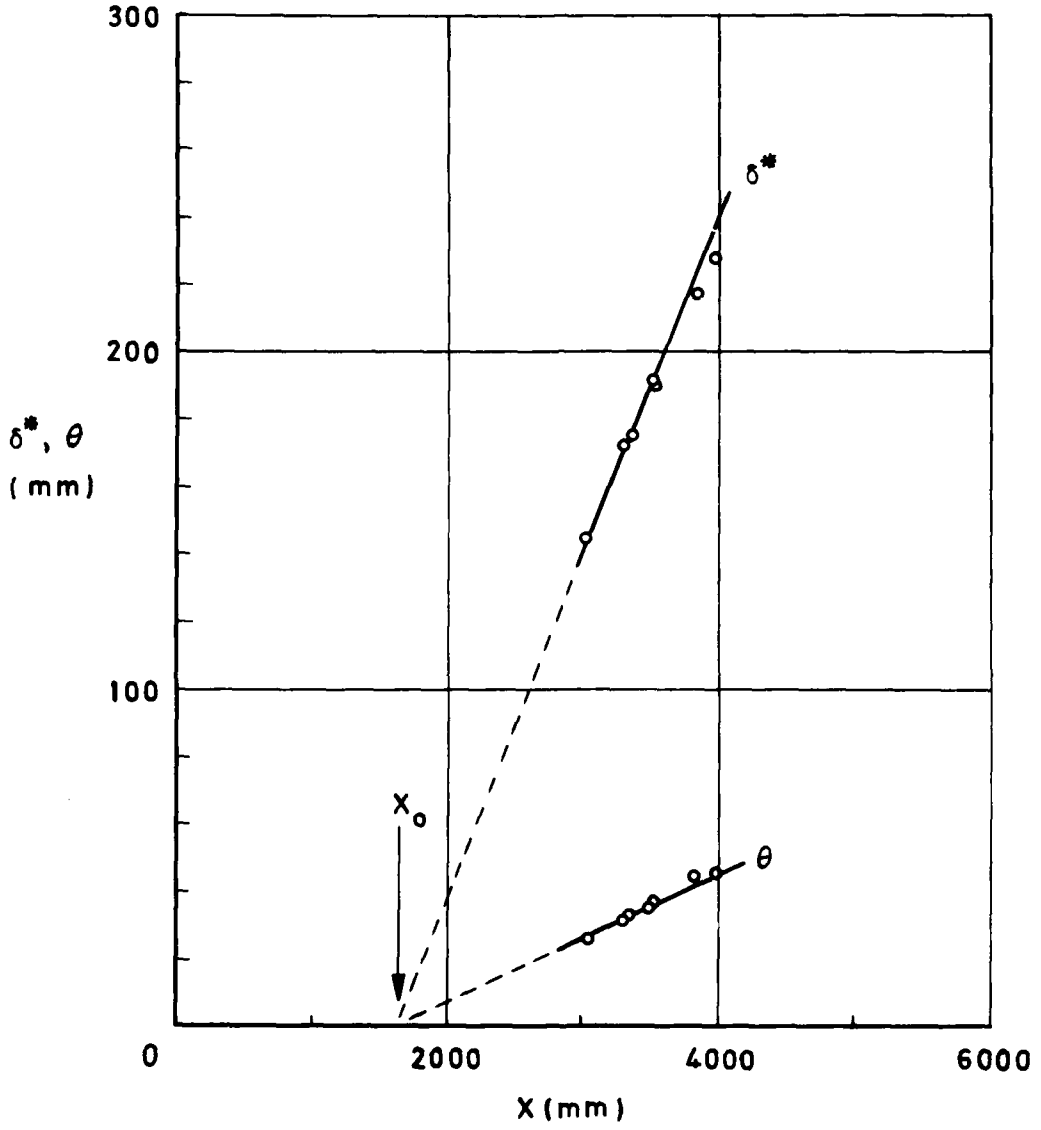

Fig 4 Growth of displacement and momentum thicknesses

Fig 5

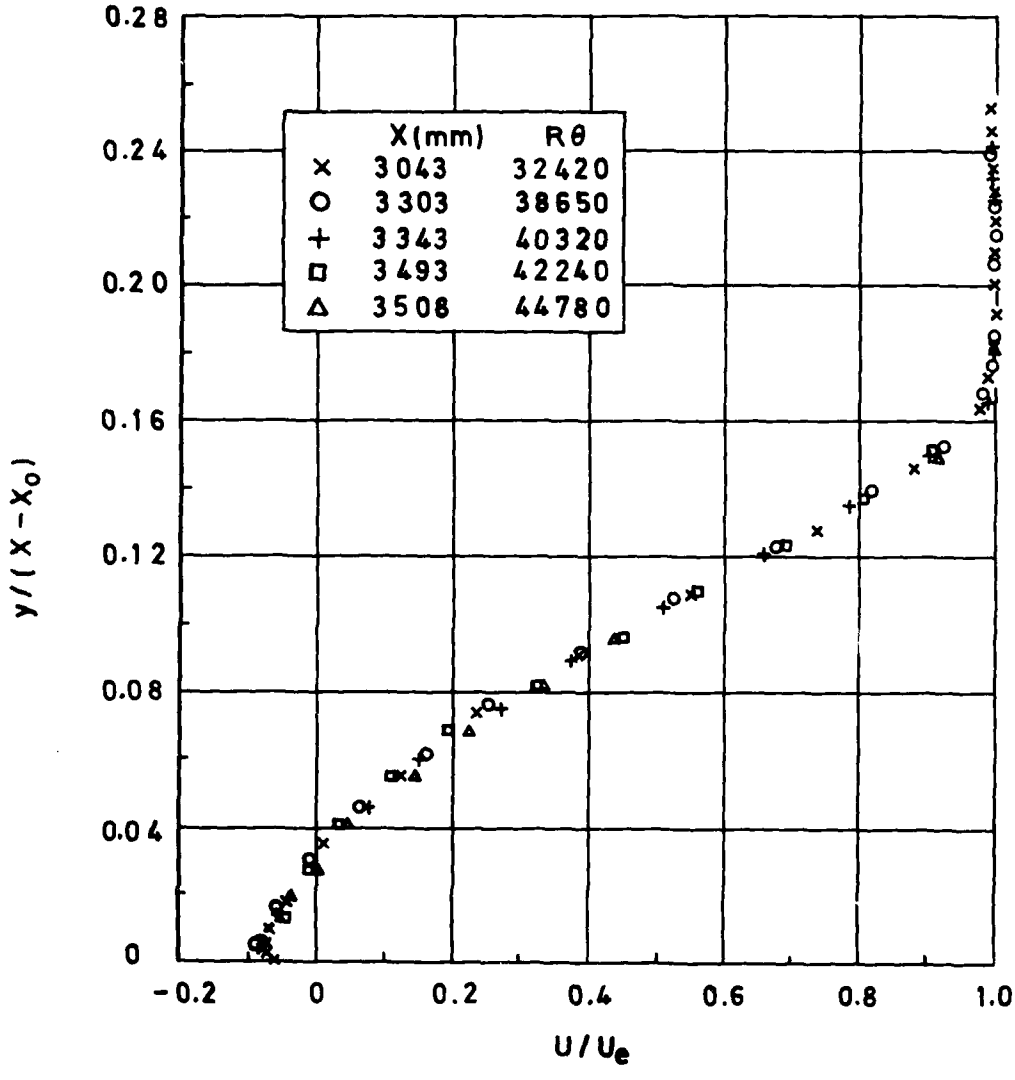

Fig 5 Normalised profiles of horizontal velocity

Fig 6

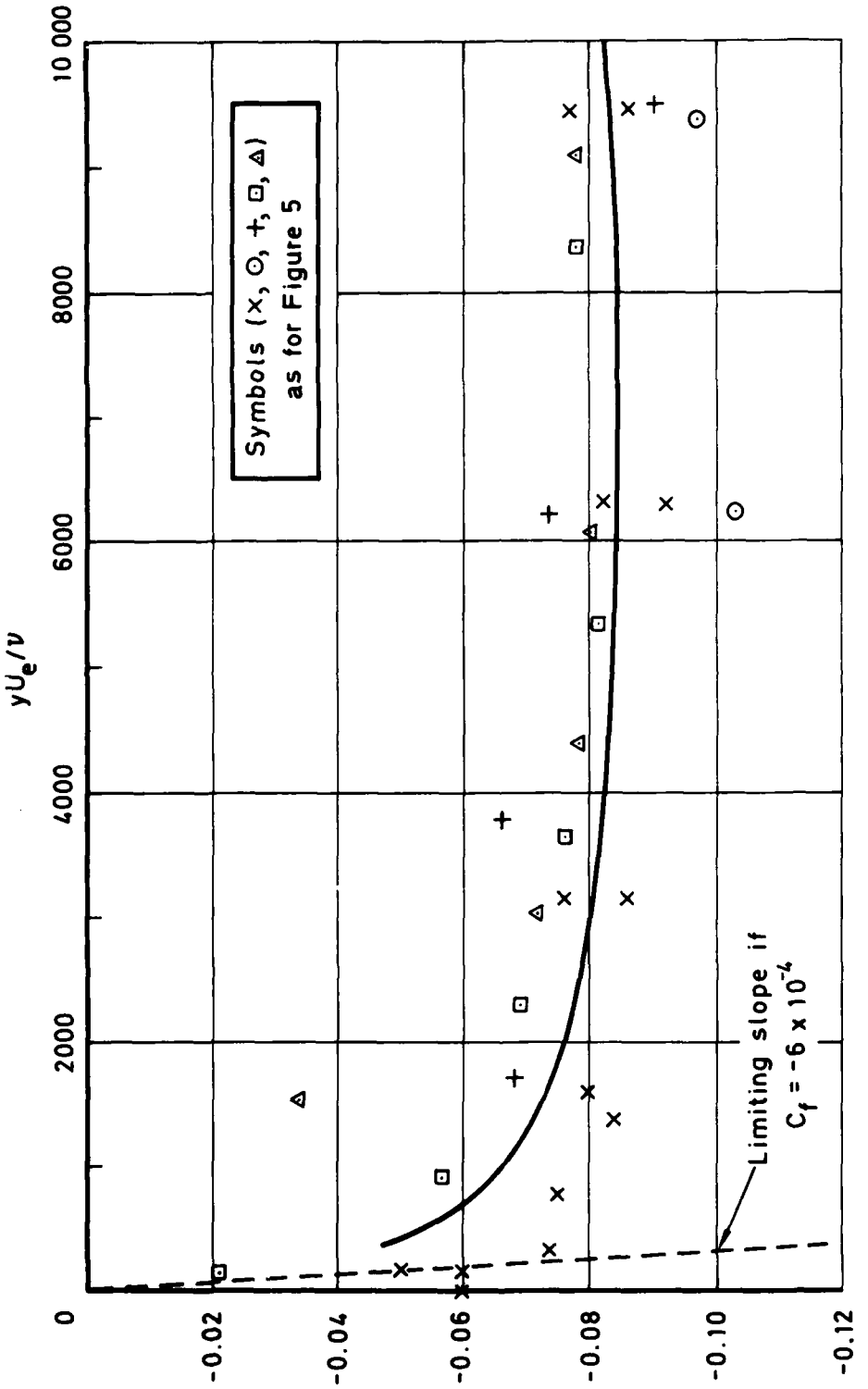

Fig 6 Horizontal velocities close to ceiling

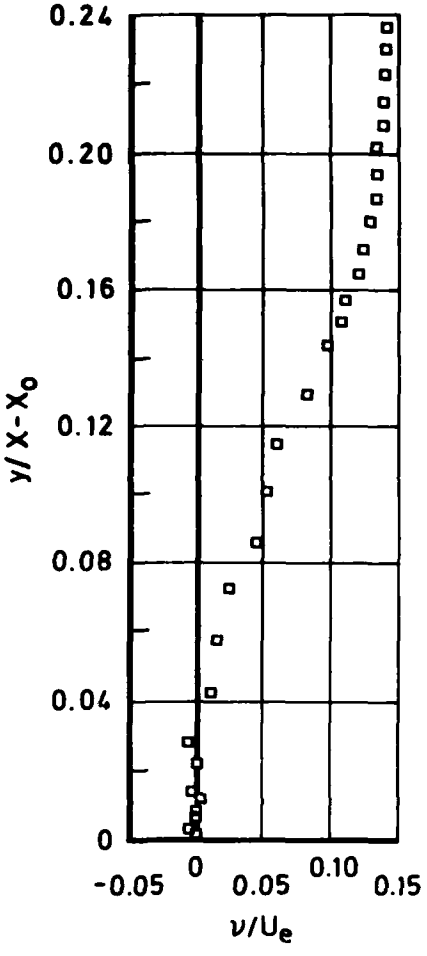

Fig 7 Vertical velocity components at X = 3343 mm

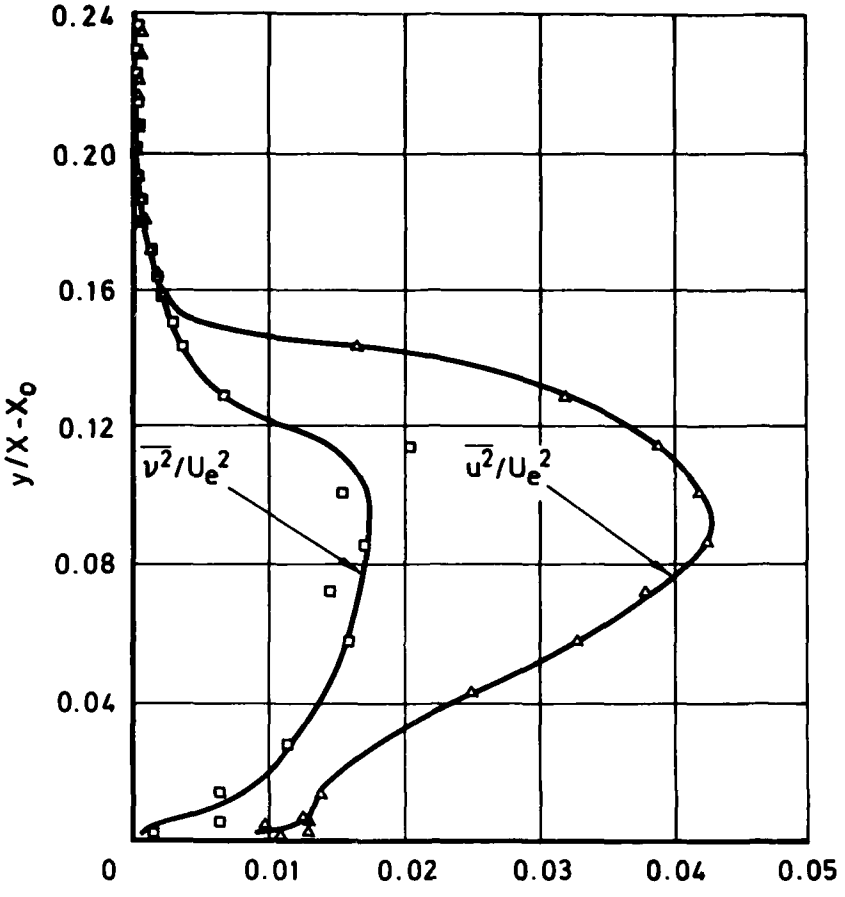

Fig 8 Mean square turbulence components at X = 3343 mm

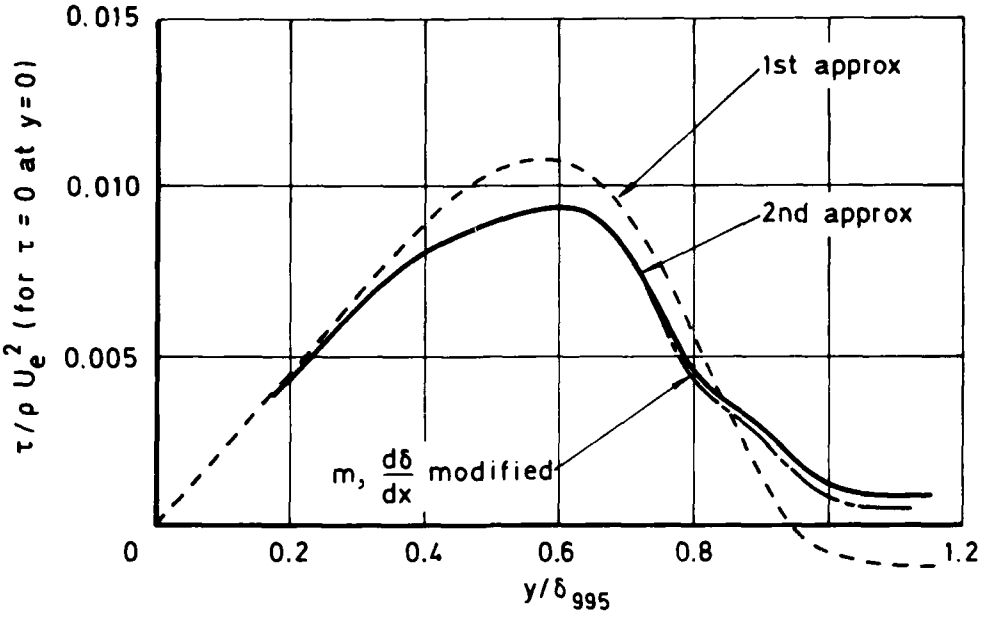

Fig 9 Shear stress estimates for separated flow

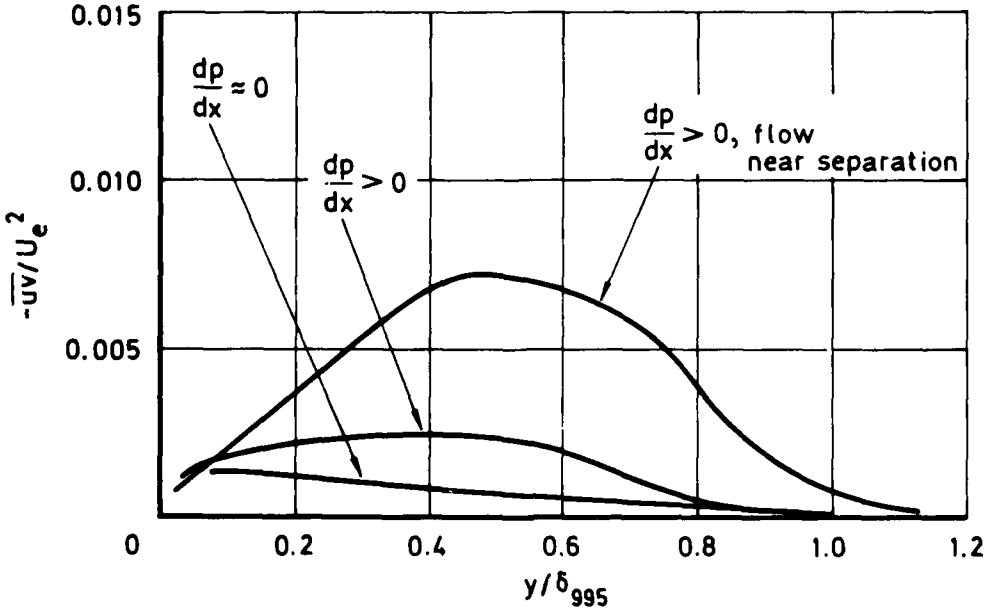

Fig 10 Shear stress distributions for equilibrium attached flow

Fig 11

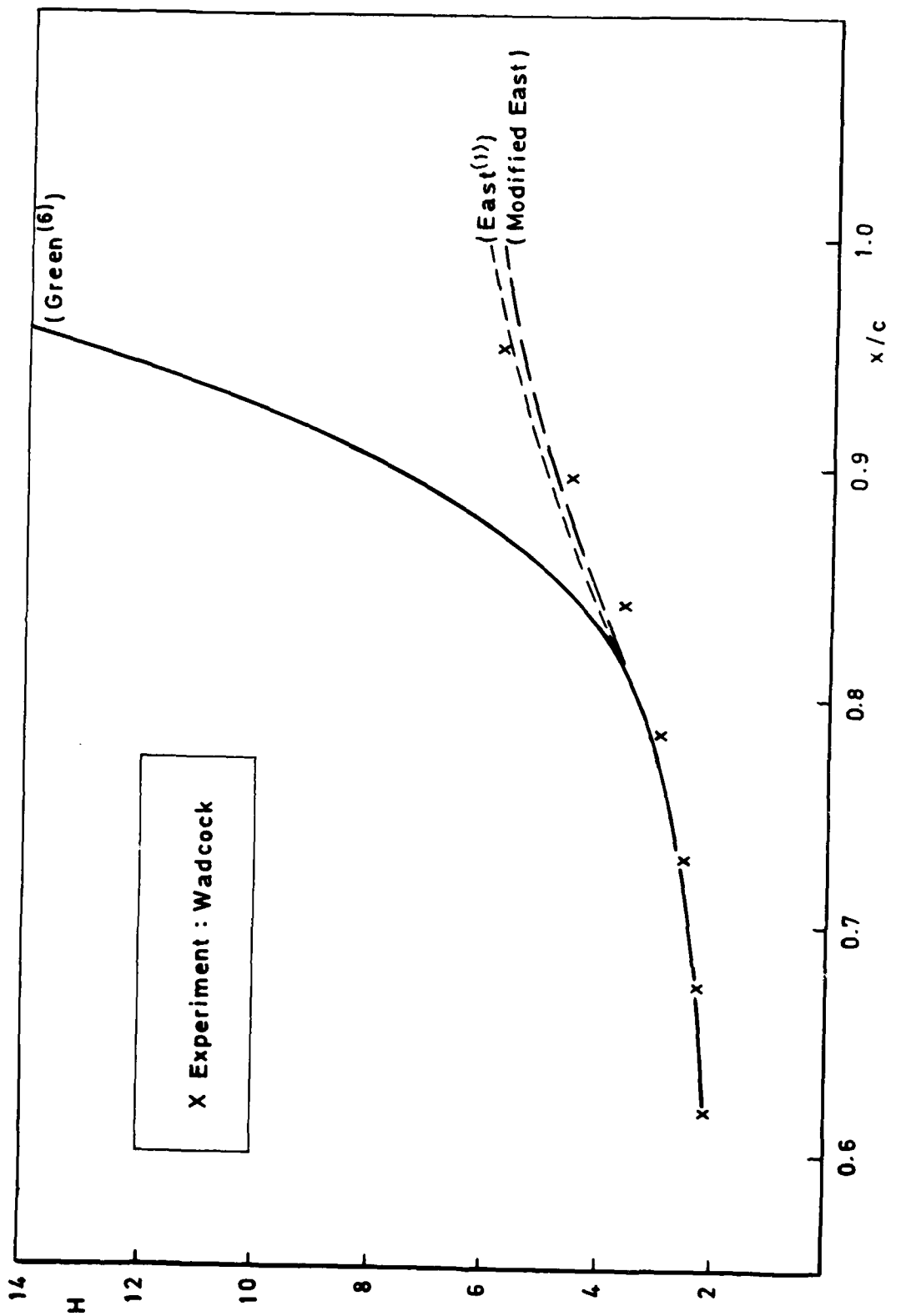

Fig 11 Measured and predicted development of H for NACA 4412:
$\alpha = 13.87^{0}$

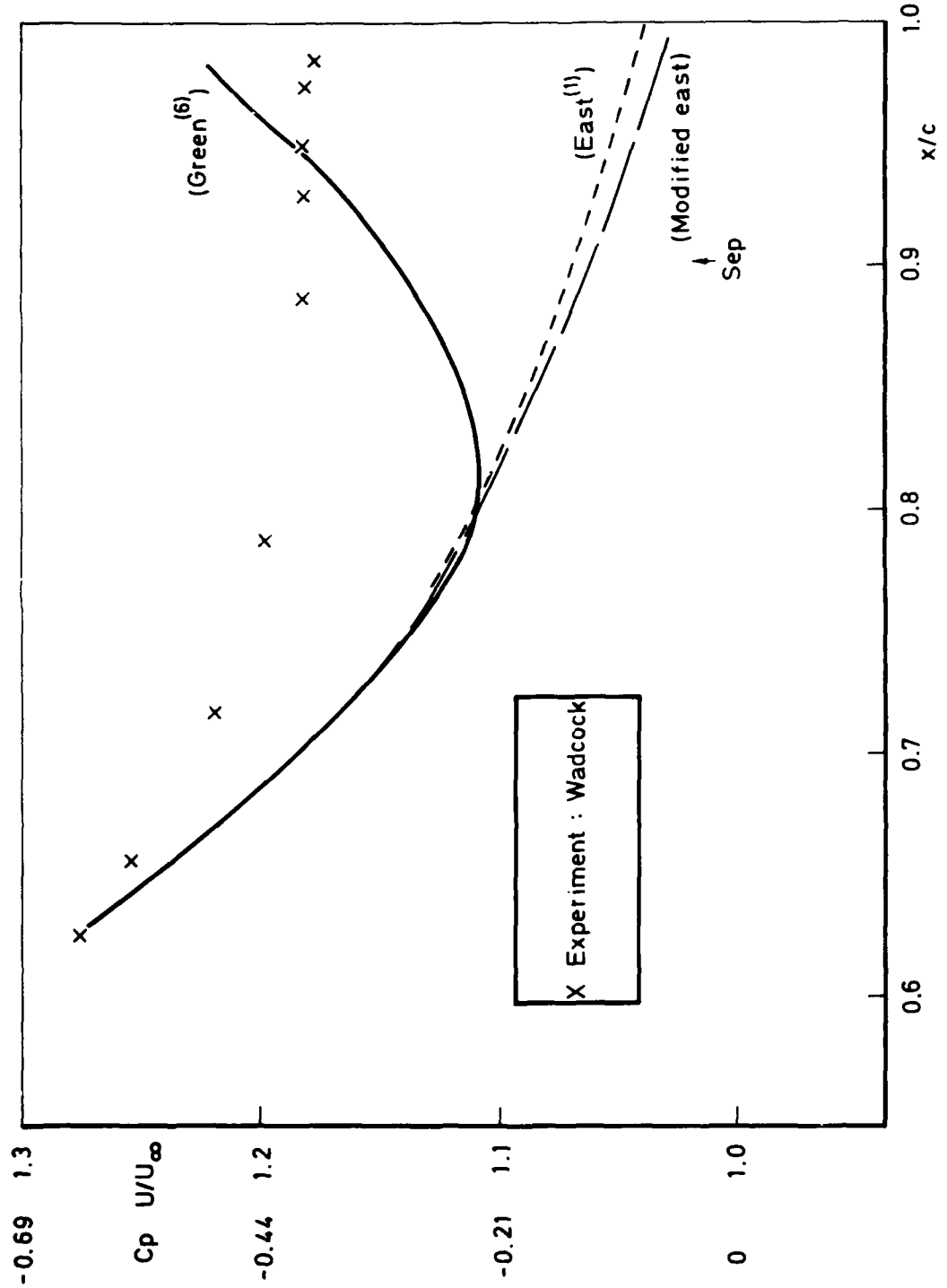

Fig 12 Measured and predicted velocity distributions for NACA 4412: $\alpha = 13.87^0$

Fig 13

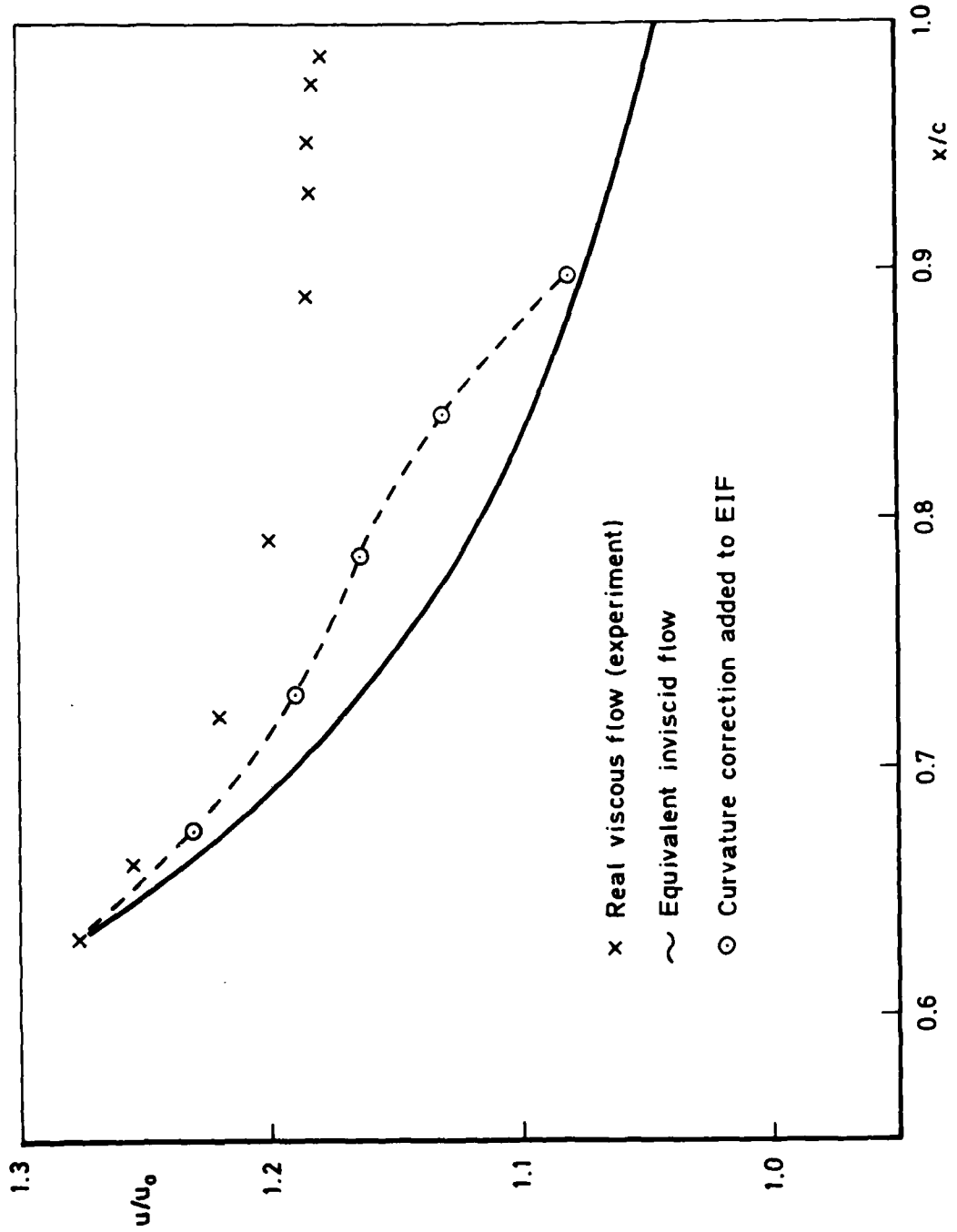

Fig 13 Curvature correction added to equivalent inviscid flow

Fig 14

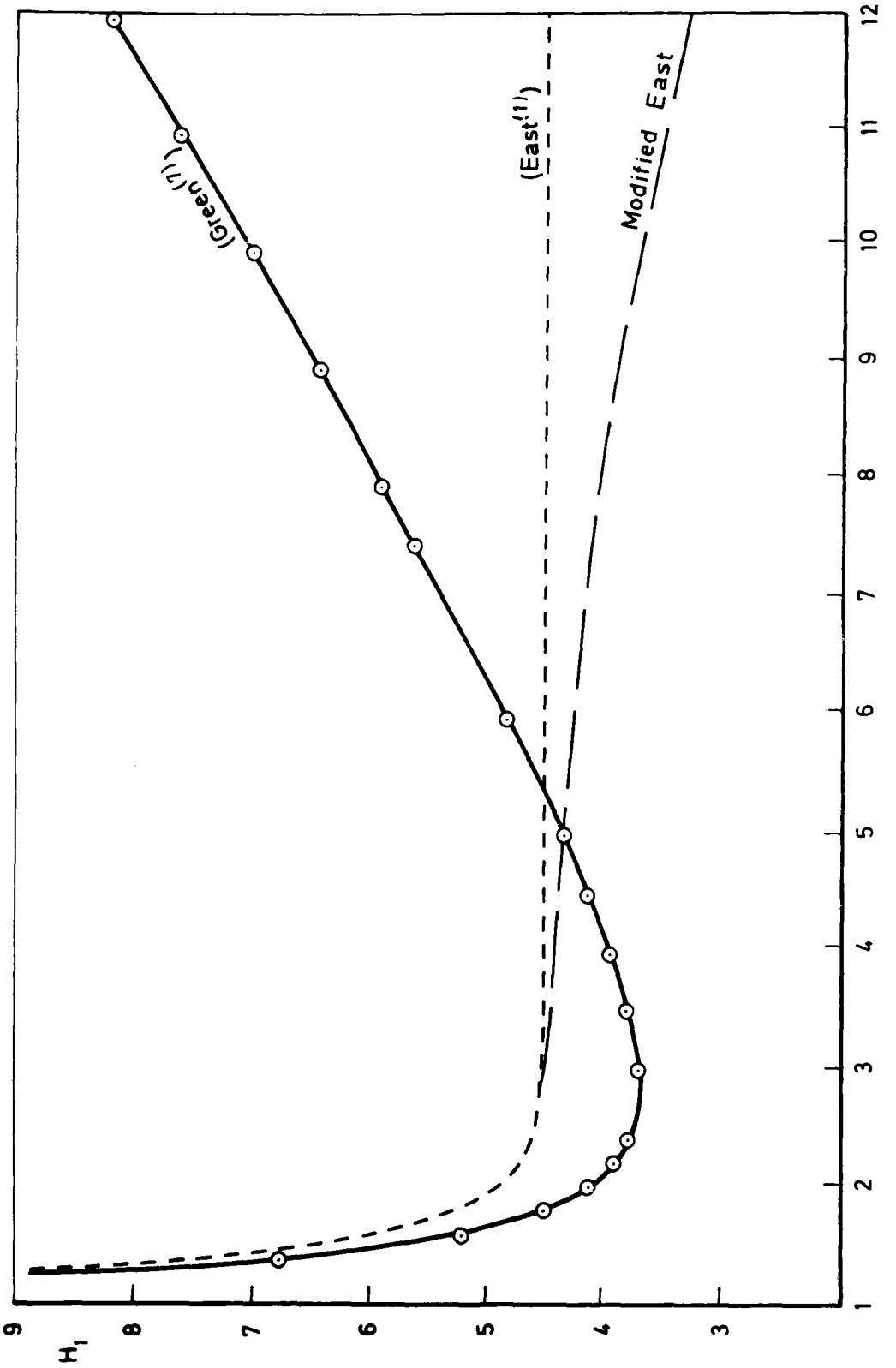

Fig 14 H - H_1 relationships used in log entrainment method

Fig 15

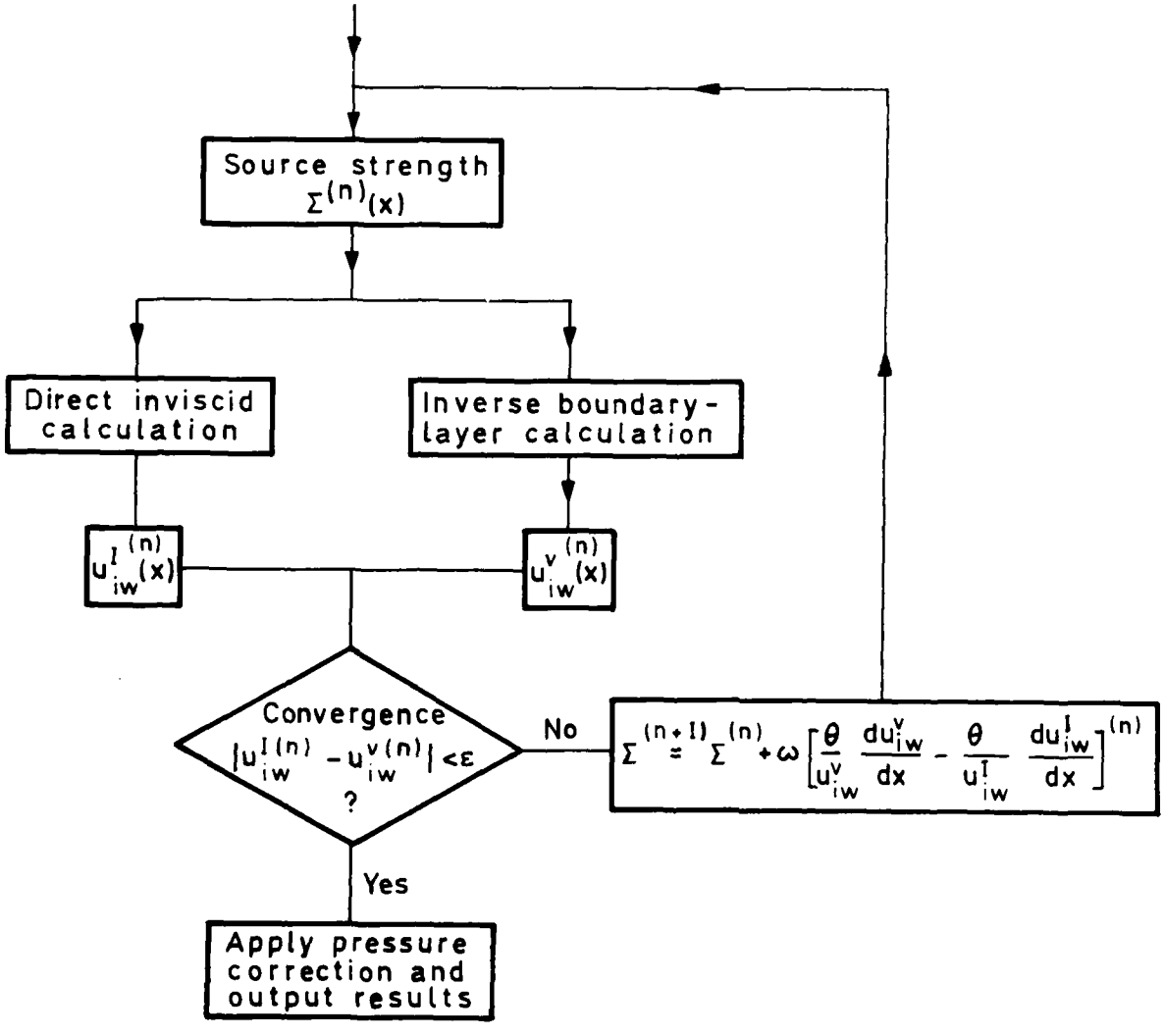

Fig 15 Flow diagram for semi-inverse scheme

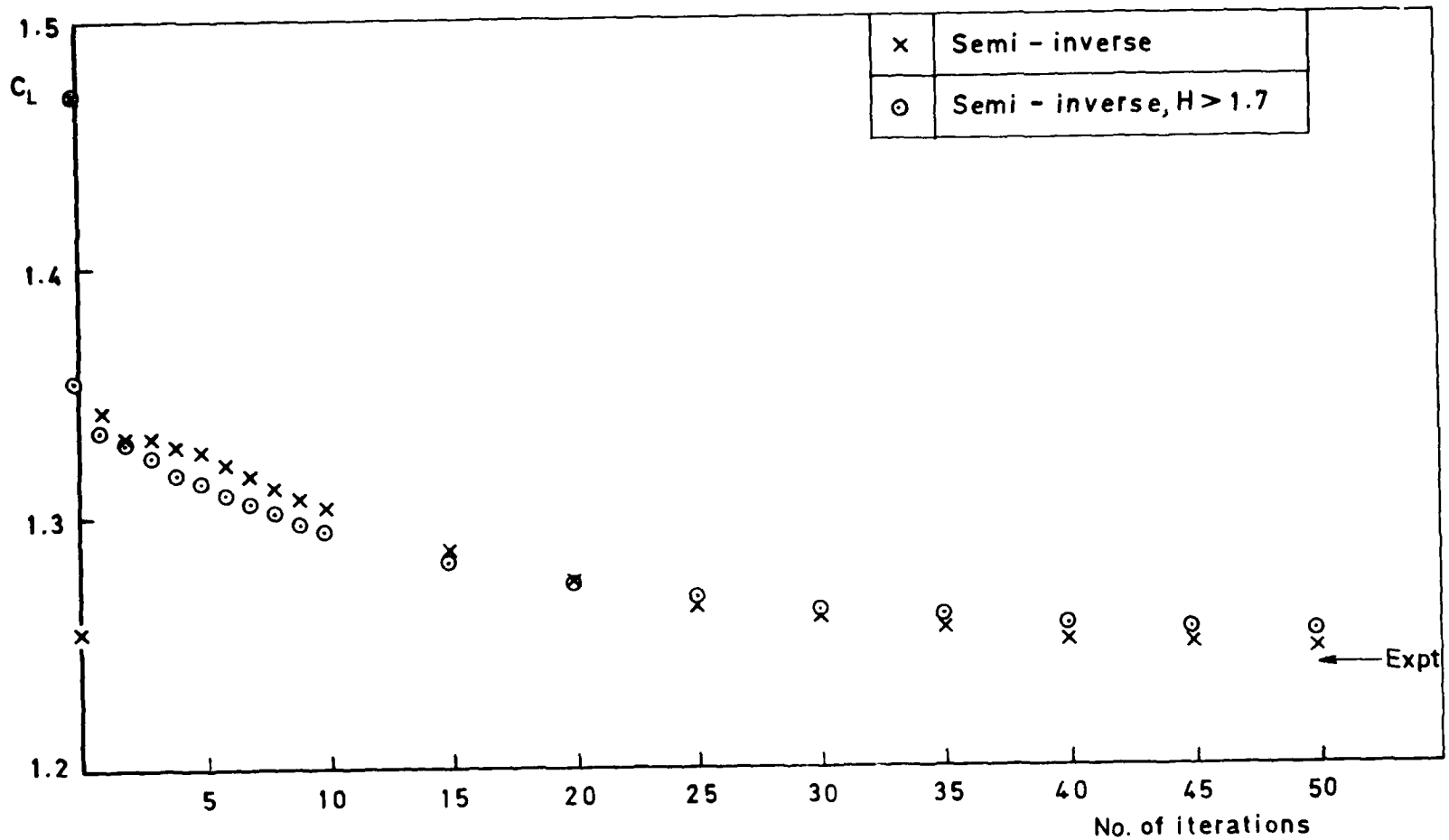

Fig 16 NACA 4412, $\alpha = 8^0$, $Re = 1.5 \times 10^6$

Fig 17

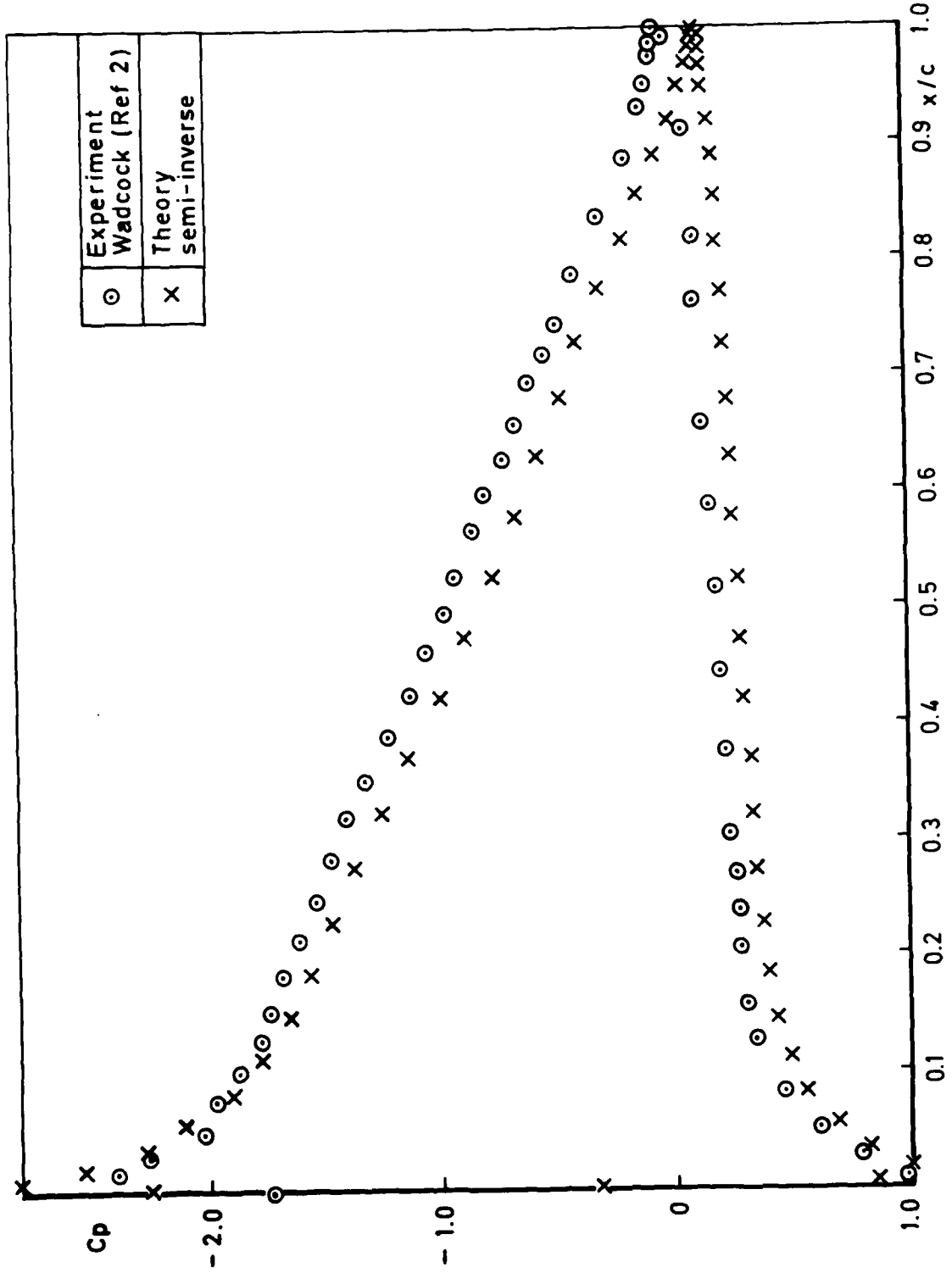

Fig 17 NACA 4412, $\alpha = 8^0$, Re = 1.5×10^6

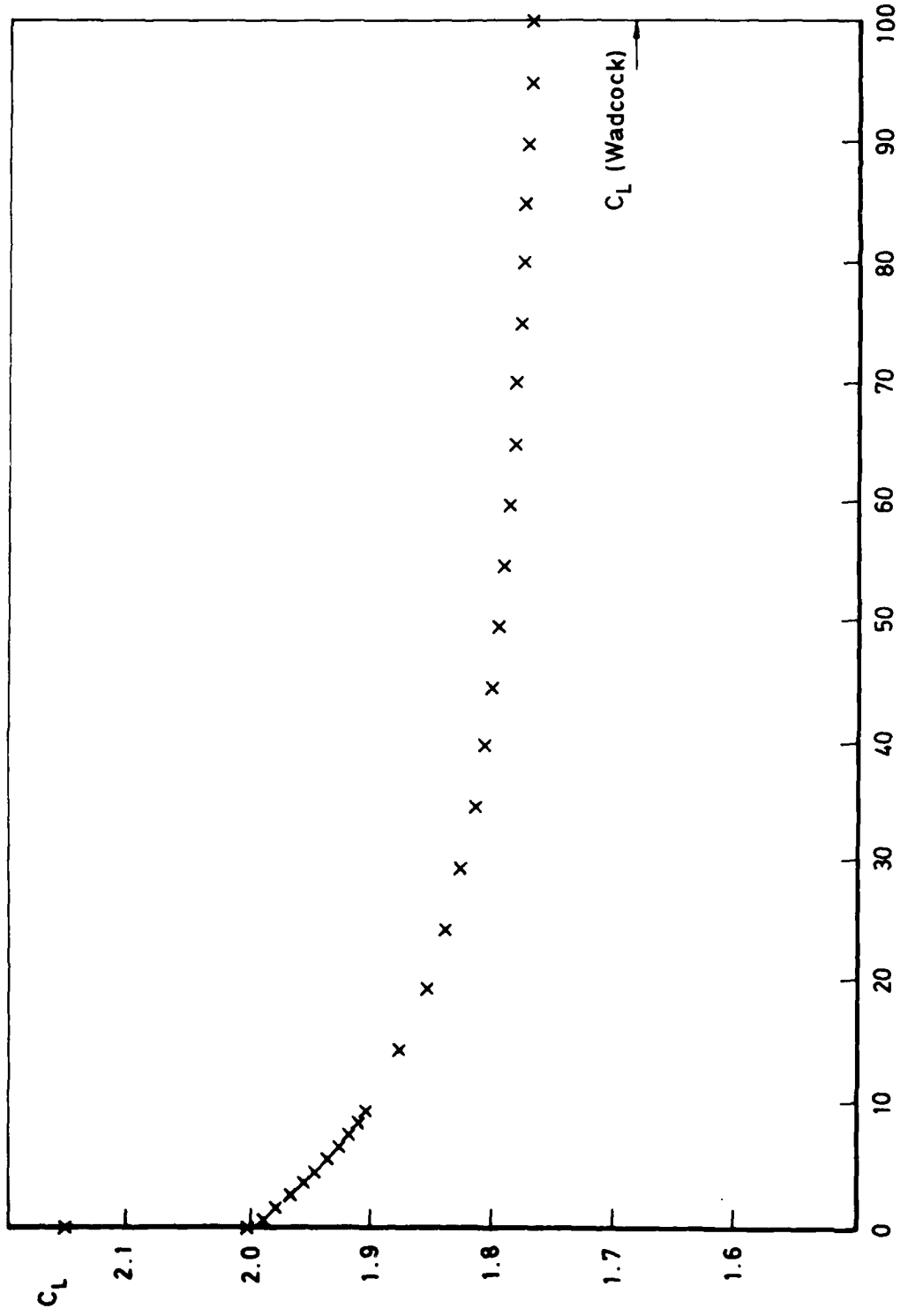

Fig 13 NACA 4412, α = 13.87°, Re = 1.5 × 10^6, transition fixed

Fig 19

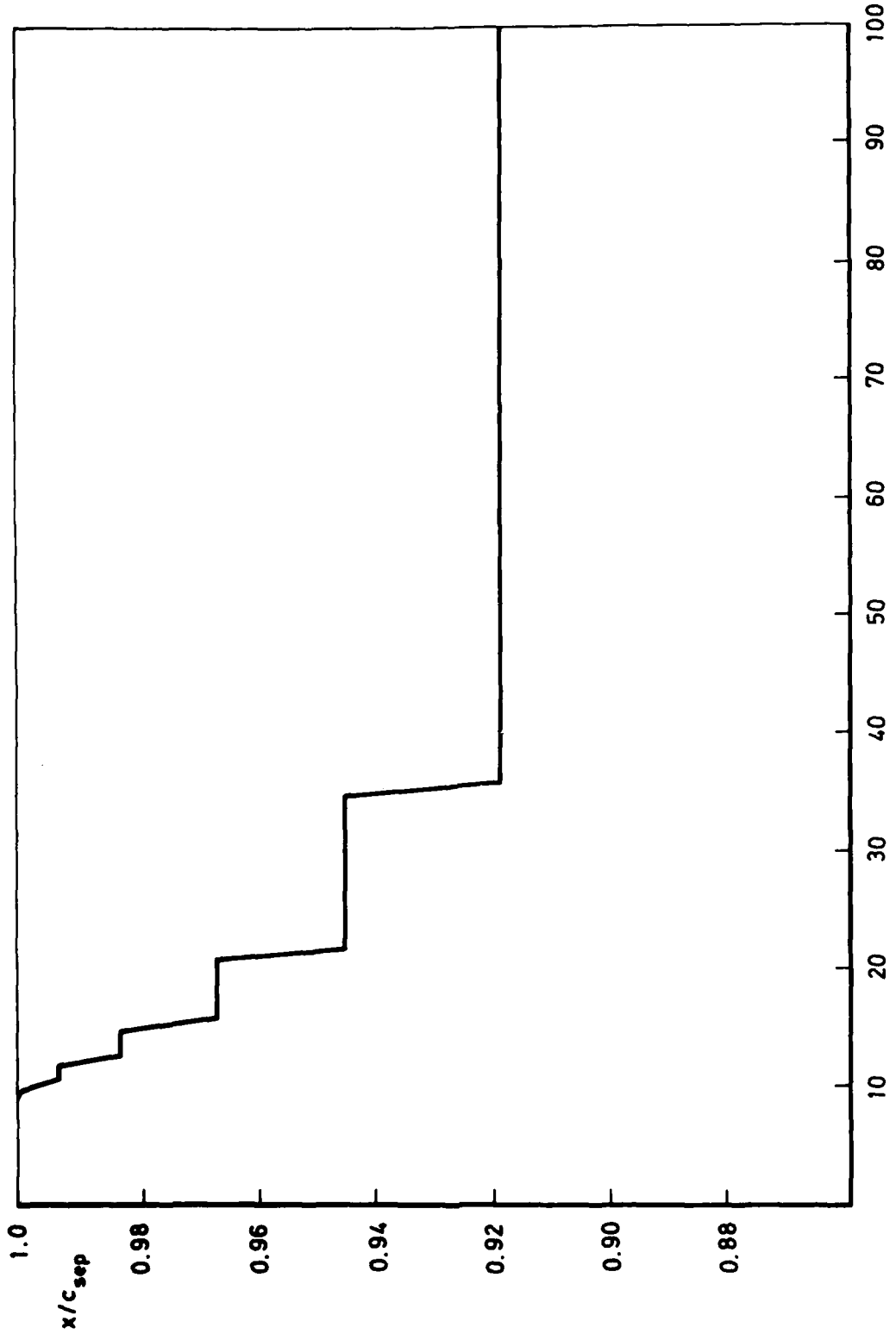

Fig 19 NACA 4412, $\alpha = 13.87^{0}$, position of separation on upper surface

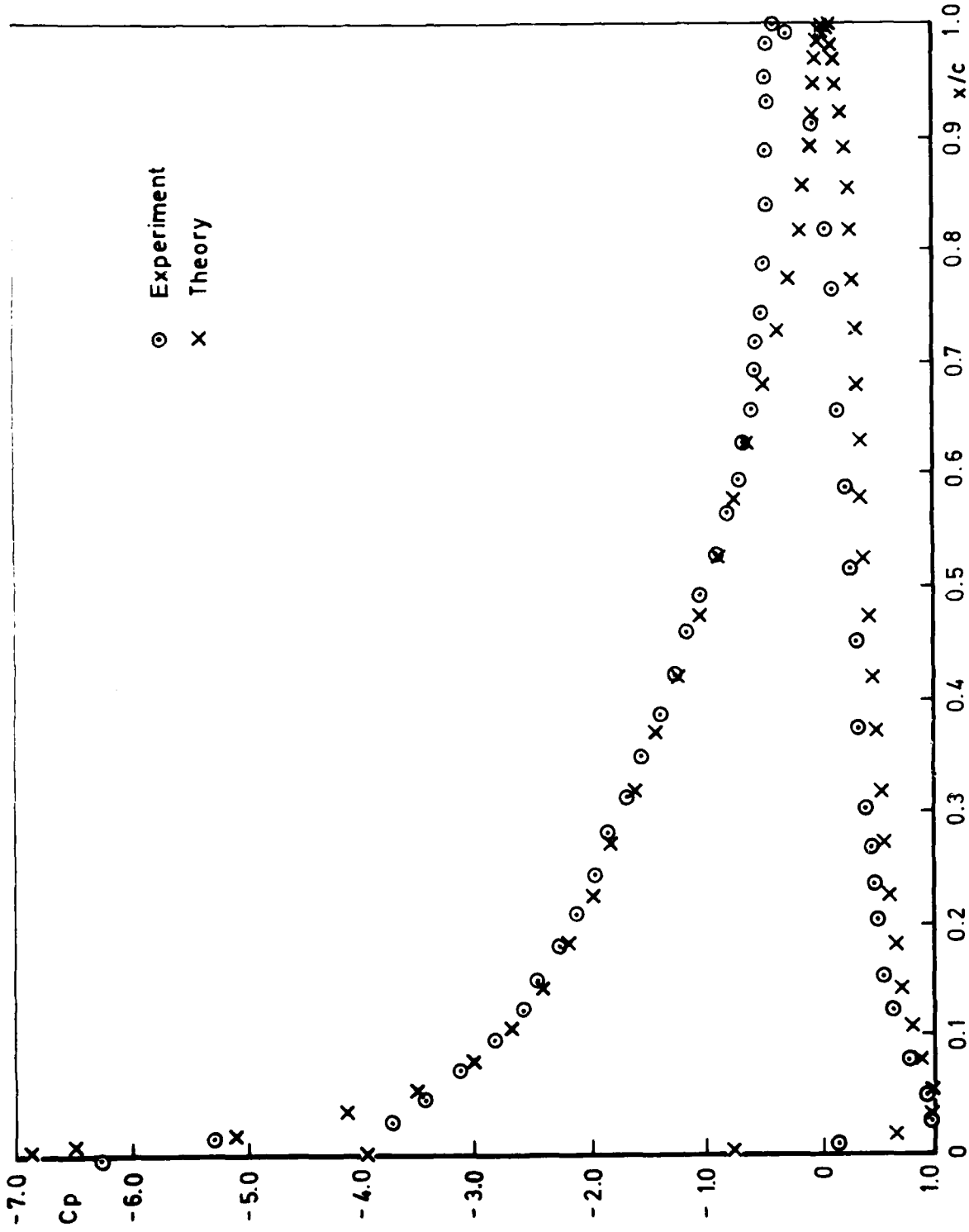

Fig 20 NACA 4412, $\alpha = 13.37^{0}$, pressure distribution

Fig 21

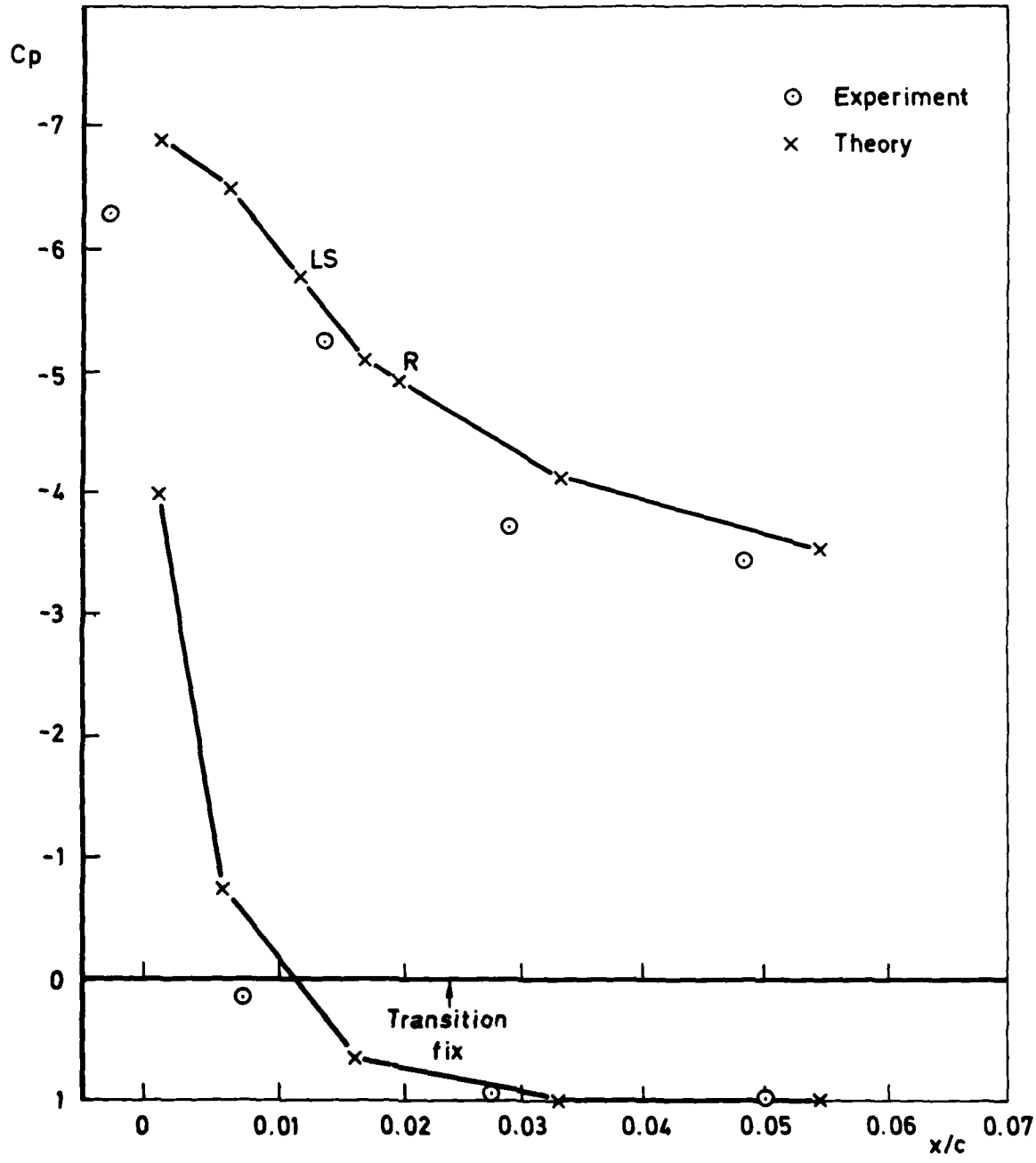

Fig 21 NACA 4412, $\alpha = 13.87^{0}$, leading edge pressure distribution

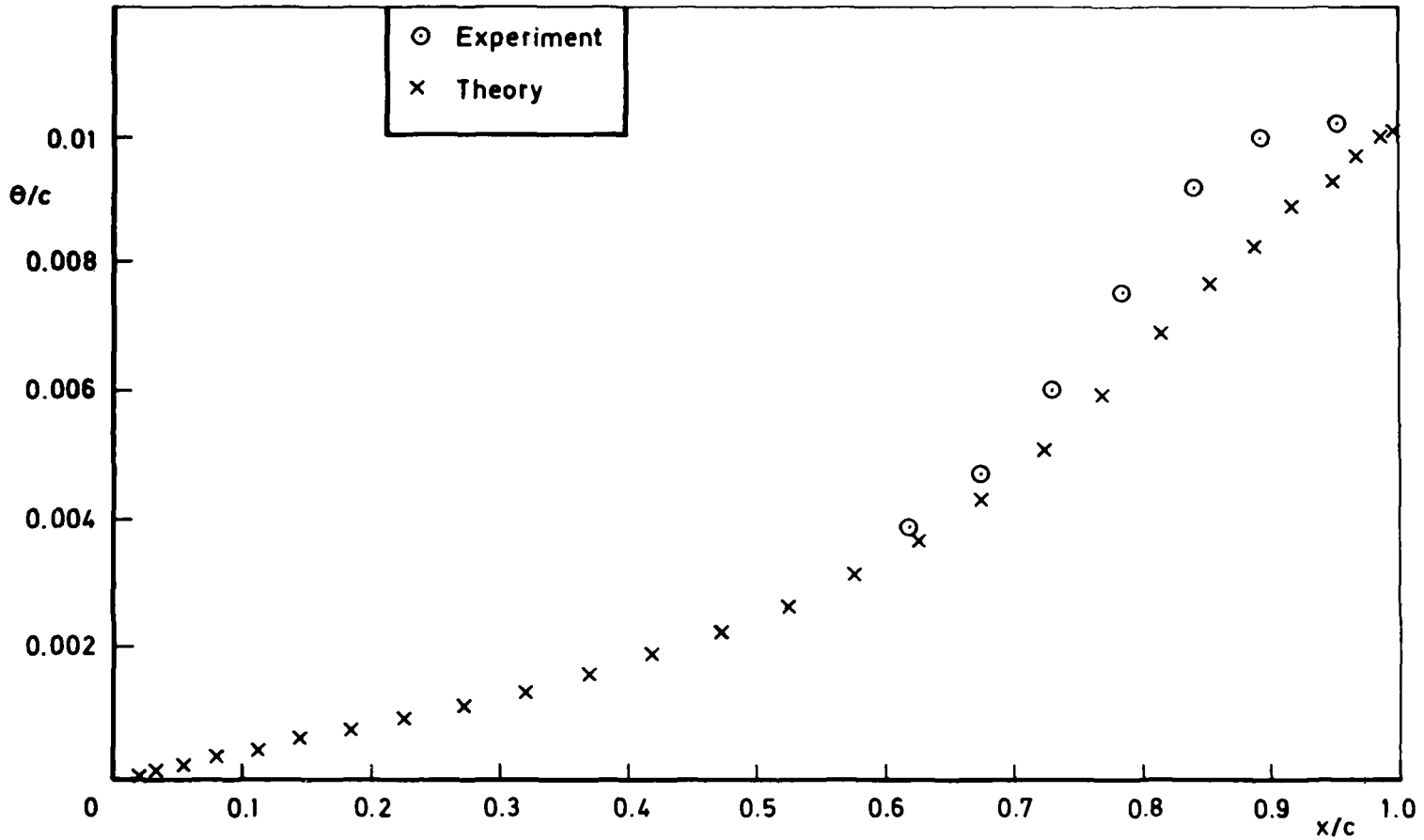

Fig 22 NACA 4412, α = 13.87°, momentum thickness on the upper surface

Fig 22

Fig 23

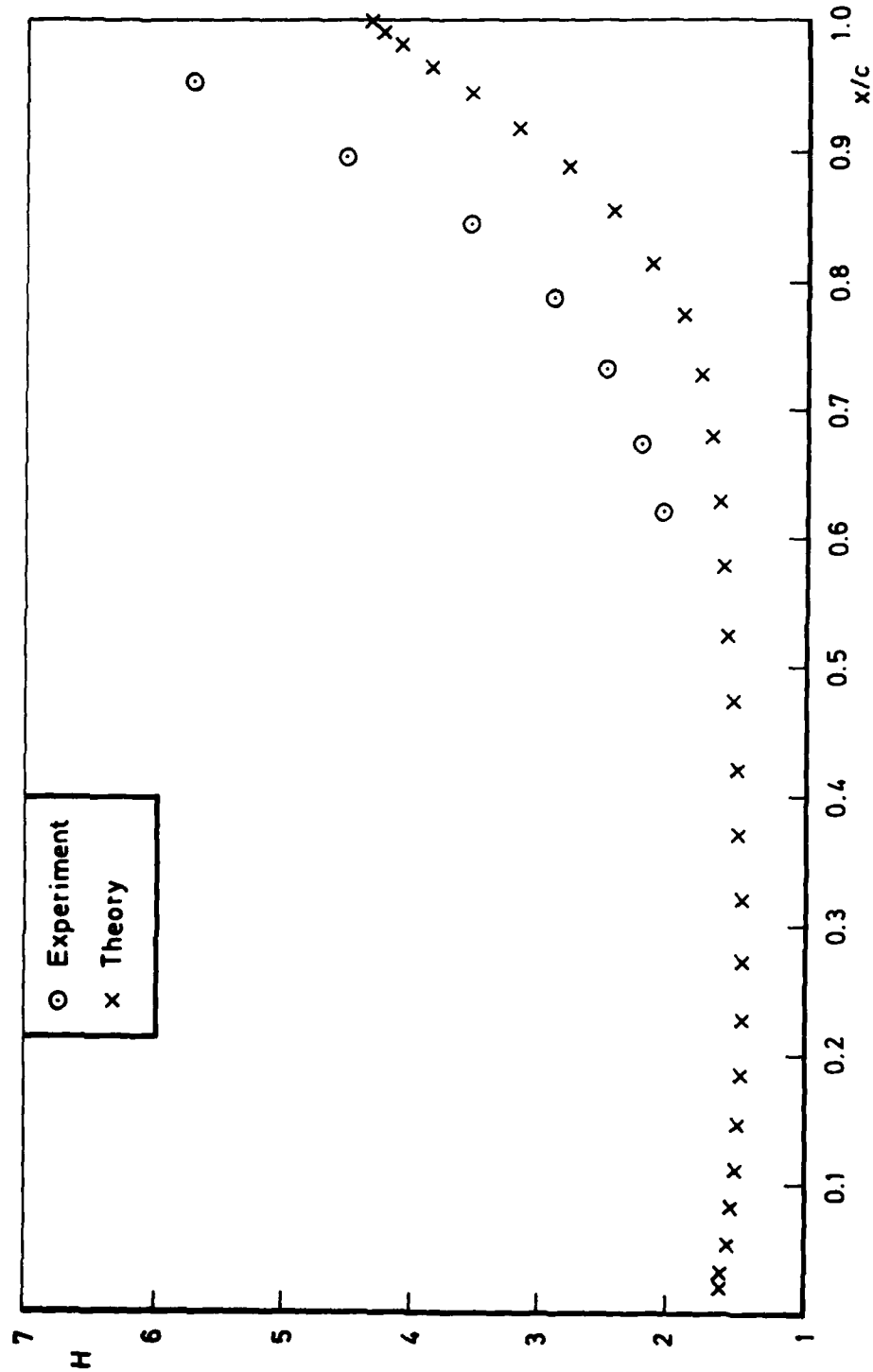

Fig 23 NACA 4412, $\alpha = 13.87^{0}$, shape parameter on the upper surface

Av 1955

REPORT DOCUMENTATION PAGE

Overall security classification of this page

UNLIMITED

As far as possible this page should contain only unclassified information. If it is necessary to enter classified information, the box above must be marked to indicate the classification, e.g. Restricted, Confidential or Secret.

1. DRIC Reference (to be added by DRIC)	2. Originator's Reference	3. Agency Reference	4. Report Security Classification/Marking
	RAE TM Aero 1955	N/A	UNLIMITED

5. DRIC Code for Originator	6. Originator (Corporate Author) Name and Location
7673000W	Royal Aircraft Establishment, Farnborough, Hants, UK
5a. Sponsoring Agency's Code	6a. Sponsoring Agency (Contract Authority) Name and Location
N/A	N/A

7. Title: Calculation and measurement of separated turbulent boundary layers

7a. (For Translations) Title in Foreign Language

7b. (For Conference Papers) Title, Place and Date of Conference

Presented at Euromech 148 "Two-dimensional separated flows" at Bochum, W. Germany, 13-15 October 1981

8. Author 1. Surname, Initials	9a. Author 2	9b. Authors 3, 4	10. Date	Pages	Refs.
Smith, P.D.	Hastings, R.C.	Williams, B.R.	October 1982	37	14

11. Contract Number	12. Period	13. Project	14. Other Reference Nos.
N/A	N/A		

15. Distribution statement

(a) Controlled by – Head of Aerodynamics Department, RAE

(b) Special limitations (if any) –

16. Descriptors (Keywords) (Descriptors marked * are selected from TEST)

Turbulent boundary layers. Separation.

17. Abstract

An inverse integral prediction method for the development of separated turbulent boundary layers developed from the lag-entrainment method is described. The inverse method uses the concept of equilibrium separated boundary layer flows and the predicted characteristics of such flows will be compared with measurements which represent the first known demonstration that equilibrium separated boundary layers can be realised experimentally.

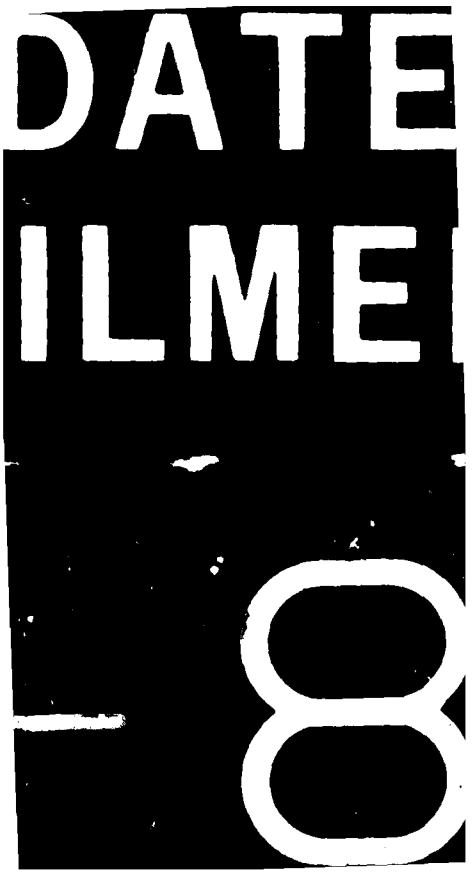
DATE
ILME
8